bioRxiv preprint doi: https://doi.org/10.1101/281931; this version posted March 13, 2018. The copyright holder for this preprint (which was not certified by peer review) is the author/funder, who has granted bioRxiv a license to display the preprint in perpetuity. It is made available under aCC-BY-NC-ND 4.0 International license.

A network of MAP-Kinase pathways and transcription factors regulates cell-to-cell communication and cell wall integrity in *Neurospora crassa*

Monika S. Fischer*, Vincent W. Wu*,†, Ji E. Lee§, Ronan C. O'Malley§, N. Louise Glass*,†,‡

*The Plant and Microbial Biology Department, The University of California, Berkeley, CA 94720-3102, †The Energy Biosciences Institute, The University of California, Berkeley , CA 94720-3102, ‡Environmental Genomics and Systems Biology Division, Lawrence Berkeley National Laboratory, Berkeley, CA 94720, §U.S. Department of Energy, Joint Genome Institute, Walnut Creek, CA 94598, USA.

NCBI Sequence Read Archive reference numbers: RNAseq data (SRP133239) and DAP-seq data (SRP133627).

bioRxiv preprint doi: https://doi.org/10.1101/281931; this version posted March 13, 2018. The copyright holder for this preprint (which was not certified by peer review) is the author/funder, who has granted bioRxiv a license to display the preprint in perpetuity. It is made available under aCC-BY-NC-ND 4.0 International license.

Short running title: ADV-1 and PP-1 in *N. crassa*

Keywords: *Neurospora crassa*, MAP Kinase, Regulatory Networks, DAP-seq, cell-to-cell communication, cell fusion

Corresponding Author

N. Louise Glass

University of California, Berkeley

Department of Plant & Microbial Biology

341A Koshland Hall

Berkeley, California 94720

510.643.2546

lglass@berkeley.edu

bioRxiv preprint doi: https://doi.org/10.1101/281931; this version posted March 13, 2018. The copyright holder for this preprint (which was not certified by peer review) is the author/funder, who has granted bioRxiv a license to display the preprint in perpetuity. It is made available under aCC-BY-NC-ND 4.0 International license.

ABSTRACT

Maintenance of cell integrity and cell-to-cell communication are fundamental biological processes. Filamentous fungi, such as *Neurospora crassa*, depend on communication to locate compatible cells, coordinate cell fusion, and establish a robust hyphal network. Two MAP-Kinase pathways are essential for communication and cell fusion in *N. crassa*; the Cell Wall Integrity/MAK-1 pathway and the MAK-2 (signal response) pathway. Previous studies have demonstrated several points of cross talk between the MAK-1 and MAK-2 pathways, which is likely necessary for coordinating chemotropic growth toward an extracellular signal, and then mediating cell fusion. Canonical MAP-Kinase pathways begin with signal reception and end with a transcriptional response. Two transcription factors, ADV-1 and PP-1, are essential for communication and cell fusion. PP-1 is the conserved target of MAK-2, while it is unclear what targets ADV-1. We did RNAseq on *Δadv-1*, *Δpp-1*, and wild-type cells and found that ADV-1 and PP-1 have a shared regulon including many genes required for communication, cell fusion, growth, development, and stress response. We identified ADV-1 and PP-1 binding sites across the genome by adapting the *in vitro* method of DNA-Affinity Purification sequencing (DAP-seq) for *N. crassa*. To elucidate the regulatory network, we misexpressed each transcription factor in each upstream MAPK deletion mutant. Misexpression of *adv-1* was sufficient to fully suppress the phenotype of the *Δpp-1* mutant and partially suppress the phenotype of the *Δmak-1* mutant. Collectively, our data demonstrate that the MAK-1-ADV-1 and MAK-2-PP-1 pathways form a tight regulatory network that maintains cell integrity and mediates communication and cell fusion.

bioRxiv preprint doi: https://doi.org/10.1101/281931; this version posted March 13, 2018. The copyright holder for this preprint (which was not certified by peer review) is the author/funder, who has granted bioRxiv a license to display the preprint in perpetuity. It is made available under aCC-BY-NC-ND 4.0 International license.

INTRODUCTION

Cell-to-cell communication is a fundamental biological process across the tree of life. There is abundant work detailing mechanisms that mediate communication processes in diverse organisms, such as quorum sensing in bacteria, neurotransmission in mammals, or pheromone sensing in *Saccharomyces cerevisiae* (Perbal 2003; Merlini *et al.* 2013). All of these systems share a general mechanism of signal release and reception that subsequently initiates specific molecular responses that often lead to changes in transcription.

Filamentous fungi, such as *Neurospora crassa*, depend on cell-to-cell communication to locate compatible cells and coordinate the process of cell fusion. *N. crassa* is a well-developed model for investigating mechanisms of cell-cell communication, chemotropic growth, and cell fusion at several points throughout the life cycle. During germination of genetically identical asexual spores, individual cells (germlings) collaborate to establish a new colony by engaging in cell-to-cell communication and chemotropic growth that ultimately results in cell fusion (Glass 2004; Fleissner *et al.* 2009; Richard *et al.* 2012; Leeder *et al.* 2013; Bastiaans *et al.* 2015). Germling fusion is an important aspect of colony establishment, and as a mature colony develops, hyphae within a colony also undergo chemotropic growth and fusion to further reinforce a robust hyphal network (Hickey *et al.* 2002). Hyphal fusion also occurs between different colonies, which is important for mediating post-fusion self/non-self recognition mechanisms and heterokaryosis (Garnjobst and Wilson 1952; Saupe 2000; Glass and Kaneko 2003; Simonin *et al.* 2012). Cell-to-cell communication and fusion are also necessary for fertilization during the process of sexual reproduction. In filamentous ascomycete species, such as *N. crassa,* fertile hyphae (trichogynes) from protoperithecia chemotropically grow towards the male

bioRxiv preprint doi: https://doi.org/10.1101/281931; this version posted March 13, 2018. The copyright holder for this preprint (which was not certified by peer review) is the author/funder, who has granted bioRxiv a license to display the preprint in perpetuity. It is made available under aCC-BY-NC-ND 4.0 International license.

gamete with the goal of cell fusion and the initiation of perithecium development, karyogamy, meiosis, and finally ascospore development (Kim and Borkovich 2004; Engh *et al.* 2010).

More than 60 genes have been identified as required for the process of germling communication and cell fusion (Fu *et al.* 2011; Read *et al.* 2012; Palma-Guerrero *et al.* 2013; Dettmann *et al.* 2014; Fleißner and Herzog 2016). Stains carrying mutations in many of the genes involved in mediating germling or hyphal fusion show a pleiotropic vegetative and female sexual development phenotype. For example, in both *N. crassa* and *Sordaria macrospora*, most fusion mutants fail to develop female reproductive structures (protoperithecia) (Engh *et al.* 2010; Fu *et al.* 2011). Some of these genes are also essential for sexual reproduction, but many are not, indicating that asexual (germling and hyphal) cell fusion is mechanistically distinct from sexual (gamete) fusion. Among the >60 known genes, there are many encoding hypothetical proteins of unknown function, but also genes/proteins in characterized pathways, including two ERK-like Mitogen Activated Protein Kinase (MAPK) pathways and pathways involved in the production of reactive oxygen species (ROS), actin organization, and calcium signaling.

Two of the three predicted MAPK pathways in *N. crassa* are required for germling communication and cell fusion (Colot *et al.* 2006; Park *et al.* 2008). In general, MAPK pathways are intermediaries that transduce information from one part of the cell (i.e. a cell-surface sensor; input) to factors in the nucleus that alter gene transcription (output). The two MAPK pathways essential for communication and cell fusion are the MAK-2 pathway, which is homologous to the pheromone response pathway in *S. cerevisiae*, and the

bioRxiv preprint doi: https://doi.org/10.1101/281931; this version posted March 13, 2018. The copyright holder for this preprint (which was not certified by peer review) is the author/funder, who has granted bioRxiv a license to display the preprint in perpetuity. It is made available under aCC-BY-NC-ND 4.0 International license.

MAK-1 pathway, which is homologous to the cell wall integrity pathway in *S. cerevisiae*. In *N. crassa,* the core conserved components of the MAK-1 pathway are MIK-1 (MAPKKK), MEK-1 (MAPKK), MAK-1 (MAPK), and SO, a scaffold important for some functions of the MAK-1 pathway (Teichert *et al.* 2014; Weichert *et al.* 2016). It is currently unknown which transcription factors are targets of the MAK-1 pathway, although transcription of several genes is dependent on MAK-1, and the rhythmic pattern of expression for a few MAK-1-dependent genes mirrors the rhythmic expression pattern of ADV-1-dependent genes (Bennett *et al.* 2013; Dekhang *et al.* 2017). Additionally, both *mak-1* and *adv-1* are targets of the circadian clock in *N. crassa* (Bennett *et al.* 2013; Dekhang *et al.* 2017). The core components of the conserved *N. crassa* MAK-2 pathway are NRC-1 (MAPKKK), MEK-2 (MAPKK), MAK-2 (MAPK), and HAM-5, a scaffold protein important during cell fusion (Dettmann *et al.* 2014; Jonkers *et al.* 2014). PP-1 is the predicted downstream transcription factor target of MAK-2; a microarray expression study demonstrated that there is overlap between MAK-2-dependent and PP-1-dependent gene expression (Leeder *et al.* 2013). Several other studies have documented cross talk between the MAK-1 and MAK-2 pathways in *N. crassa* and in other filamentous ascomycete fungi, some of which is mediated by the STRIPAK complex (Maerz *et al.* 2008; Maddi *et al.* 2012; Dettmann *et al.* 2012, 2013; Leeder *et al.* 2013; Fu *et al.* 2014).

Transcription is a common point of regulation for biological processes, and two conserved transcription factors in *N. crassa* (ADV-1 and PP-1) are essential for germling communication and fusion. Both the *Δadv-1* and *Δpp-1* deletion mutants have a pleiotropic phenotype and were initially identified as female-sterile mutants (Li 2005; Colot *et al.* 2006; Fu *et al.* 2011). PP-1 is a C2H2 zinc finger transcription factor that is

bioRxiv preprint doi: https://doi.org/10.1101/281931; this version posted March 13, 2018. The copyright holder for this preprint (which was not certified by peer review) is the author/funder, who has granted bioRxiv a license to display the preprint in perpetuity. It is made available under aCC-BY-NC-ND 4.0 International license.

124 homologous to the *S. cerevisiae* pheromone response pathway transcription factor, *STE12*
125 (Leeder *et al.* 2013). The core component of this pathway in *S. cerevisiae* is the Fus3p
126 MAPK cascade, that once activated, leads to de-repression of Ste12p (Merlini *et al.* 2013).
127 Ste12-like proteins, including PP-1, have two C2H2-Zn^{2+} motifs and a homeobox-like
128 STE domain involved in binding DNA (Errede and Ammerer 1989). In *N. crassa* the STE
129 domain is essential for PP-1 function, but the C2H2-Zn^{2+} motifs are dispensable (Leeder
130 *et al.* 2013). Ste12-like transcription factors in fungi are regulated by direct
131 phosphorylation and phosphorylation of associated regulatory proteins (Blackwell *et al.*
132 2007). Several phosphorylation sites have been identified on PP-1 in *N. crassa*, but the
133 biological significance of these sites remains unknown (Leeder *et al.* 2013; Xiong *et al.*
134 2014; Jonkers *et al.* 2014).
135
136 ADV-1 is a $Zn(II)_2Cys_6$ transcription factor that, like PP-1, regulates growth, and asexual
137 and sexual development. ADV-1 is not as broadly conserved as PP-1, and clear *adv-1*
138 homologs are restricted to the filamentous Ascomycete species (Pezizomycotina). In the
139 self-fertile (homothallic) species *S. macrospora*, the *adv-1*-ortholog, *pro1*, is required for
140 protoperithecial development, while heterothallic *N. crassa* does not require *adv-1* for
141 protoperithecia development (Masloff *et al.* 1999). In *N. crassa*, *adv-1* is essential for post-
142 mating perithecial development, asexual cell fusion, and wild-type-like growth rate. Both
143 ADV-1 and Pro1 have a GAL4-like DNA-binding domain and a transcription-activation
144 domain. In contrast to the *S. cerevisiae* protein GAL4p, Pro1 lacks a coiled-coil
145 dimerization domain, indicating that Pro1 (and ADV-1) likely function independently
146 (Masloff *et al.* 2002). Unlike PP-1, upstream factors that influence ADV-1 regulated
147 transcription are largely unknown, with the exception of a ChIPseq experiment that

bioRxiv preprint doi: https://doi.org/10.1101/281931; this version posted March 13, 2018. The copyright holder for this preprint (which was not certified by peer review) is the author/funder, who has granted bioRxiv a license to display the preprint in perpetuity. It is made available under aCC-BY-NC-ND 4.0 International license.

148 identified *adv-1* as a target of the circadian clock master regulator, the White Collar
149 Complex (Smith *et al.* 2010). ADV-1 is essential for developmental oscillations (i.e.
150 conidiation) and the quantity of *adv-1* mRNA and ADV-1 protein oscillates with the clock
151 (Smith *et al.* 2010). Furthermore, the expression of ADV-1 target genes in a mature
152 colony matches the rhythm of other clock-controlled genes. These data led to the
153 hypothesis that hyphal fusion is a clock-regulated developmental process (Dekhang *et al.*
154 2017).
155
156 The *Δadv-1* and *Δpp-1* mutants share many phenotypes across filamentous fungi, yet the
157 relationship between these two transcription factors remains unclear. Independent
158 expression profiling studies investigating ADV-1 or PP-1-dependent transcription indicate
159 that at least some genes require ADV-1 and PP-1 for wild type levels of expression (Li
160 2005; Nowrousian *et al.* 2007; Leeder *et al.* 2013; Dekhang *et al.* 2017). Here, we
161 compared expression profiles using RNAseq on *Δadv-1* and *Δpp-1* germlings relative to
162 expression patterns in wild-type germlings. To identify genes that were regulated and
163 bound by ADV-1 or PP-1, we developed an *in vitro* method for identifying transcription
164 factor binding sites in *N. crassa* and other fungi called DNA Affinity Purification
165 sequencing (DAP-seq). DAP-seq is similar to ChIPseq, except that *in vitro* synthesized
166 transcription factors are incubated with native genomic DNA. DNA fragments bound by
167 the transcription factor are then identified by high throughput sequencing methods.
168 DAP-seq has been used in a global analysis of transcription factor binding sites in
169 *Arabidopsis thaliana* (O'Malley *et al.* 2016). Our data showed that PP-1 directly regulates
170 *adv*-1; ADV-1 is the primary regulator of many genes that are important for asexual

bioRxiv preprint doi: https://doi.org/10.1101/281931; this version posted March 13, 2018. The copyright holder for this preprint (which was not certified by peer review) is the author/funder, who has granted bioRxiv a license to display the preprint in perpetuity. It is made available under aCC-BY-NC-ND 4.0 International license.

171 growth, cell fusion and development. To investigate the linkage between *mak-1*, *mak-2*,
172 *adv-1*, and *pp-1*, we used misexpression and phenotypic analyses. Our data showed that
173 *mak-1* primarily functions upstream of *adv-1*, and *mak-2* primarily functions upstream of
174 *pp-1*. However, the MAK-1/ADV-1 pathway and the MAK-2/PP-1 pathway engage in
175 crosstalk and both pathways form a regulatory network that mediates growth,
176 communication, fusion, and the response to cell wall stress.
177

178 **MATERIALS & METHODS**

179 RNA isolation

180 Strains used: FGSC 2489 (wild-type), FGSC 11042 (*Δadv-1*) and *Δpp-1* (Leeder *et al.*
181 2013). Each strain was initially grown on Vogel's Minimal Medium (VMM) (Vogel 1956)
182 agar slant tubes for 5 days. Conidia harvested, filtered through cheesecloth, and then
183 inoculated into 100mL of liquid VMM in a 250mL flask to a final concentration of
184 10^6conidia/mL. Flasks were incubated at 30°C in constant light for 2.5 hours shaking at
185 220 rpm to induce germination, followed by 2.5 hours stationary incubation to allow
186 communication to occur. *Δpp-1* conidia have slightly delayed germination, thus these
187 conidia were shaken for 3 hours, followed by 2.5 hours stationary incubation. Germlings
188 were harvested by vacuum filtration over nitrocellulose paper and transferred to a 2mL
189 screw cap tube that was immediately frozen with liquid N_2. Experimental design for each
190 strain: conidia from one VMM slant tube was used to inoculate 8 flasks of liquid VMM,
191 then two flasks were pooled during germling harvest, resulting in a total of 4 samples per
192 strain. RNA was extracted using a previously described TRIzol-based method (Leeder *et*
193 *al.* 2013). RNA quality and concentration were quantified via Bioanalyzer at the qb3

bioRxiv preprint doi: https://doi.org/10.1101/281931; this version posted March 13, 2018. The copyright holder for this preprint (which was not certified by peer review) is the author/funder, who has granted bioRxiv a license to display the preprint in perpetuity. It is made available under aCC-BY-NC-ND 4.0 International license.

facility at UC Berkeley. Three samples per strain with the highest quality and concentration of RNA were submitted for library prep and sequencing on an Illumina HiSeq3000 at the UC Davis DNA Technologies Core.

RNAseq data analysis and visualization

Fast-X Toolkit (http:// hannonlab.cshl.edu/fastx_toolkit/index.html) was used to filter out low quality raw reads (~11-12% of all reads) and Tophat (Langmead *et al.* 2009) mapped high quality reads to the *N. crassa* transcriptome version 12 (ftp://ftp.broadinstitute.org/pub/annotation/fungi/neurospora_crassa/assembly/NC12) Differential expression was calculated using three independent methods: Cuffdiff (Roberts *et al.* 2010), DESeq2 (Love *et al.* 2014), and EdgeR (Robinson *et al.* 2010; McCarthy *et al.* 2012). We defined the threshold for significant differential expression to be $-2 < \log_2\text{FoldChange} < 2$ and p.adj<0.01. RNAseq raw data (.fastq) is available at the NCBI Sequence Read Archive with accession number SRP133239.

We used the Circos data visualization tool (Krzywinski *et al.* 2009) to generate Figure 2. Genes are grouped according to known function or predicted function based on homology (BLASTp, FungiDB, or the Broad Institute's Fungal Orthogroups Repository v1.1). Highlighted gene ID's indicate genes that have an ADV-1 binding site or a PP-1 binding site 2kb upstream from the start codon. PP-1 binding sites were identified solely via DAP-seq, whereas ADV-1 binding sites are the consensus between DAP-seq data and a previously published ChIPseq dataset (Dekhang *et al.* 2017).

Genomic DNA Library Preparation

bioRxiv preprint doi: https://doi.org/10.1101/281931; this version posted March 13, 2018. The copyright holder for this preprint (which was not certified by peer review) is the author/funder, who has granted bioRxiv a license to display the preprint in perpetuity. It is made available under aCC-BY-NC-ND 4.0 International license.

DAP-seq was originally developed for *A. thaliana* (O'Malley *et al.* 2016). Here we adapted the protocol in O'Malley *et al* for use with *N. crassa*. FGSC 2489 was grown in liquid VMM for 24 hours at 25˚C and shaking at 220rpm. Mycelia were harvested using vacuum filtration over Whatman #1 filter papers, and transferred into 2ml tubes for flash freezing in liquid N_2. Cells were ruptured by bead beating for 1 minute with 1mm silica beads and DNA lysis buffer (0.05M NaOH, 1mM EDTA, 1% TritonX) was added to each sample tube. DNA was purified using DNeasy Blood & Tissue kit (Qiagen Inc.), and sheared to 300bp peak using Covaris LE220 sonicator. AMPure XP beads were used to remove DNA above and below target molecular weight. Initially, sheared DNA was mixed in with AMPure XP beads (in PEG-8000) at a ratio of 100:60. At this ratio, beads bind DNA with molecular weight above 700bp. Supernatant from this primary binding was taken and added to new beads where final ratio of DNA solution to PEG-8000 was at 100:90. At this ratio, DNA below ~300bp do not bind to AMPure XP beads, and remaining DNA was be eluted for library preparation. KAPA library kit for illumina sequencing was used to prepare final libraries and stored at -20˚C for later use.

Transcription factor cloning, transcription, translation and DNA Affinity Purification (DAP)

TF open reading frames (ORF) were amplified from cDNA using RNA to cDNA ecodry premix (Clonetech). Amplified TFs sequences were inserted into pIX *in vitro* expression vector modified to contain an N-termainl HALO-Tag (O'Malley *et al.* 2016). Vector backbone was amplified and assembled with TF ORFs using Gibson assembly and then transformed into competent *E. coli* cells for storage and production.

bioRxiv preprint doi: https://doi.org/10.1101/281931; this version posted March 13, 2018. The copyright holder for this preprint (which was not certified by peer review) is the author/funder, who has granted bioRxiv a license to display the preprint in perpetuity. It is made available under aCC-BY-NC-ND 4.0 International license.

In vitro transcription and translation of TFs was achieved by using Promega TnT T7 Rabbit Reticulocyte Quick Coupled Transcription/Translation System. 1μg of plasmid DNA, 60μl of TnT Master Mix, and 1.5μl of 1mM methionine were combined and incubated overnight at room temperature. Expression was verified using Western blot analysis with Promega HaloTag monoclonal antibody. Completed TnT reactions were incubated with 20ng of genomic DNA library, 1μg salmon sperm for blocking, and 20μl Promega Magne HaloTag Beads on a rotator for 1 hour at room temperature. Bead bound proteins and protein bound DNA were washed three times with 2.5% Tween20 in PBS. HaloTag beads were resuspended in 30μl ddH_2O and heated to 98˚C for 10 minutes to denature protein and release DNA fragments into solution. Supernatant was transferred to a new tube for PCR amplification. DNA was amplified for final libraries using KAPA Hifi polymerase for 12-16 cycles of PCR.

DAP-seq data analysis

Filtered reads were mapped against *N. crassa* OR74A genome (v12) using bowtie2 v2.3.2 (Kim *et al.* 2013). SamTools (Li *et al.* 2009) was used to convert .sam to .bam files and to create .bai index files for viewing reads on IGV (Integrated Genomics Viewer). MACS2 (Zhang *et al.* 2008) with p-value cutoff at 0.001 was used for calling peaks. A negative control data set consisting of DAP pull-down with Promega TnT master mix with no plasmid added, salmon sperm, and genomic DNA was also input into MACS2 as the control condition. We repeated the ADV-1 DAP-seq once and pooled the results of both DAP-seq runs. DAP-seq data is available at the NCBI Sequence Read Archive with accession number SRP133627.

bioRxiv preprint doi: https://doi.org/10.1101/281931; this version posted March 13, 2018. The copyright holder for this preprint (which was not certified by peer review) is the author/funder, who has granted bioRxiv a license to display the preprint in perpetuity. It is made available under aCC-BY-NC-ND 4.0 International license.

265

266 Motif construction

267 To construct biologically meaningful transcription factor DNA binding motifs, we used
268 DAP-seq peaks associated with differentially expressed genes according to corresponding
269 RNAseq data. Sequences of these true positive peaks were collected using a custom
270 python script that reads in genomic position of each peak from the MACS2 output file,
271 and ascertains the sequence from *N. crassa* OR74A Broad v12 genome FASTA file. The
272 script output is a FASTA file with sequences from all true positive peaks. Output FASTA
273 files were input into MEME or DREME v4.12.0 with flags maxw =20, minsites = 5,
274 nmotifs = 8, denoting max width of motif, minimum number of sites for each motif and
275 number of motifs to generate respectively. For ADV-1 specifically, we used set of 41 DAP
276 binding peak sequences. These peaks were within the promoter regions of from genes that
277 fit two parameters: within 1kbp upstream of the ATG start site according to DAP-seq, as
278 well as 4 fold down-regulated in the Δ*adv-1* mutant as compared to wild-type. Nucleotide
279 sequences for these 41 peaks were fed into MEME v4.12.0 to build the ADV-1 binding
280 motif. For PP-1, we loosened the parameters slightly to 2 fold down-regulated in *Δpp-1* as
281 compared to wild-type, due to the small number of genes both directly bound according
282 to DAP-seq and differentially expressed at a 4 fold level. Nucleotide sequences for 22
283 peaks were fed into MEME v4.12.0 to build the PP-1 binding motif.

284

285 qRT-PCR

286 Germlings were prepared and RNA extracted as described for RNAseq samples. qRT-
287 PCR reactions were prepared following the manufacturer protocols for the Bioline
288 SensiFast™ SYBR® no-ROX One-Step kit and Bio-Rad CFX Connect™ Real-Time

bioRxiv preprint doi: https://doi.org/10.1101/281931; this version posted March 13, 2018. The copyright holder for this preprint (which was not certified by peer review) is the author/funder, who has granted bioRxiv a license to display the preprint in perpetuity. It is made available under aCC-BY-NC-ND 4.0 International license.

289 PCR Detection System. Each sample was replicated at least 4 times within a 96-well-plate
290 and total reaction volume was 20μL. Expression data was normalized to both actin and
291 wild-type following the $2^{-\Delta\Delta Ct}$ method (Livak and Schmittgen 2001).
292
293 Strain construction
294 Misexpression strains were made by transforming the *his-3*-targeted vectors described
295 below into *his-3*$^{-}$ deletion strains as previously described (Colot *et al.* 2006). Positive
296 transformants were selected for histidine prototrophy and hygromycin resistance. To
297 avoid any off-target affects that may have resulted from the transformation process, we
298 backcrossed each transformant to *his-3* (FGSC 9716 or FGSC 6103). Transformants that
299 were incapable of going through a cross were purified via microconidial isolation (Pandit
300 and Maheshwari 1994). All genotypes were confirmed via PCR.
301
302 The *Ptef1-adv-1-v5 his-3* vector was constructed by amplifying *adv-1* from genomic DNA
303 with primers that omitted the native STOP codon and added *Xba*I and *Pac*I cut sites on
304 either end of the *adv-1* ORF. PCR products were gel purified and blunt ligated into
305 pCR®-Blunt. The *adv-1* sequence was ligated into an in-house vector containing V5
306 using *Xba*I and *Pac*I sites. *adv-1-v5* was amplified using a reverse primer that added a
307 TGA stop codon at the end of the V5 sequence, in addition to *Eco*RI and *Apa*I cut sites.
308 This PCR product was gel purified and blunt ligated into pCR®-Blunt, digested and
309 ligated into an in-house vector based on pMF272 (Freitag *et al.* 2004) containing the *tef-1*
310 promoter (*Ptef1*) using *Xba*I and *Apa*I cut sites. The *Ptef1-pp-1-v5* vector was constructed by
311 amplifying *pp-1* from the *Pccg1-pp-1-gfp his-3* vector (Leeder *et al.* 2013) with primers that

bioRxiv preprint doi: https://doi.org/10.1101/281931; this version posted March 13, 2018. The copyright holder for this preprint (which was not certified by peer review) is the author/funder, who has granted bioRxiv a license to display the preprint in perpetuity. It is made available under aCC-BY-NC-ND 4.0 International license.

312 added *Bam*HI and *Pac*I sites. This PCR product was ligated into pCR®-Blunt, digested
313 and ligated into the *Ptef1-adv1-V5 his3* vector using *Bam*HI and *Pac*I cut sites, which
314 resulted in replacement of the *adv-1* sequence with *pp-1* coding sequences. The sequence
315 of *Ptef1-adv1-v5* and *Ptef1-pp-1-v5* in the *his-3* vectors was confirmed via Sanger
316 sequencing prior to transforming into *his3*$^{-}$ deletion strains.
317
318 Growth, fusion, mating, and cell wall stress assays
319 Standard *N. crassa* growth conditions, media, and protocols are available at
320 http://www.fgsc.net/Neurospora/NeurosporaProtocolGuide.htm. For assays to quantify
321 aerial hyphae height, growth rate, and germling communication, conidia were grown up
322 and harvested as described for RNAseq. Conidial suspensions were diluted to specified
323 concentrations and immediately used for phenotyping assays. Aerial hyphae were grown
324 up from 10^6 conidia in 1mL of liquid VMM, incubated at 30°C in the dark for 72 hrs
325 (n=6). Growth rate was measured by inoculating 100µL of 10^6conidia/mL onto one end
326 of a glass race tube containing 25mL of VMM 1.5% agar. Linear growth in race tubes
327 was measured every 24 hrs for at least 4 days (n=3). Germling communication assays
328 consisted of spreading 300µL of 10^7conidia/mL on a 9 cm VMM 1.5% agar plate. Plates
329 were incubated at 30°C in the dark for 3.5hours. To visualize germlings, agar squares
330 (~1cm^2) were excised and observed with a Zeiss Axioskop 2 equipped with a Q Imaging
331 Retiga-2000R camera (Surrey) using a 40x/1.30 Plan-Neofluar oil immersion objective
332 and the iVision Mac4.5 software (Heller *et al.* 2016). Germling communication frequency
333 was determined with the ImageJ Cell Counter tool (http://imagej.nih.gov/ij/). For
334 mating assays, female strains were inoculated onto Synthetic Cross (SC) agar 5.4cm plates

bioRxiv preprint doi: https://doi.org/10.1101/281931; this version posted March 13, 2018. The copyright holder for this preprint (which was not certified by peer review) is the author/funder, who has granted bioRxiv a license to display the preprint in perpetuity. It is made available under aCC-BY-NC-ND 4.0 International license.

(Westergaard and Mitchell 1947). These plates were incubated at 30°C in the dark for two days, and then moved to 25°C and light for an additional 5 days to allow for full production of protoperithecia. Male strains were grown up on VMM as described above. Mating was initiated by inoculating female plates with 150μL of un-diluted conidial suspension of male strains of the opposite mating type. Cell wall stress assays were conducted on large petri plates containing 45mL of VMM with 1.5% agar and 2% FGS. The following cell wall stress drugs were added and mixed to VMM+FGS immediately prior to pouring each plate (one drug/plate): 1.3μg/mL Caspofungin, 1.5mg/mL Calcofluor White, and 1mg/mL Congo Red. Conidia for cell wall stress tests were grown up and harvested as described above, then diluted to 10^6spores/mL. A 1:5 dilution series was prepared starting with 10^6spore/mL as the most concentrated dilution. Conidial solutions were then spotted onto freshly poured plates at 5μL/spot.

RESULTS

ADV-1 and PP-1 have a shared regulon in germlings

To investigate the how ADV-1 (NCU07392) and PP-1 (NCU00340) regulate germling communication and fusion, we compared expression profiles of *Δadv-1, Δpp-1*, and wild-type germlings. We extracted RNA from germlings 2.5 hours after germination, which is when the majority of wild-type germlings were actively engaging in chemotropic growth and cell fusion (Figure 1A). Our RNAseq data confirm previous studies that implicated PP-1 and ADV-1 as transcriptional activators (Masloff *et al.* 2002; Leeder *et al.* 2013). Figure 1B illustrates that the vast majority of differentially expressed genes were down regulated in *Δadv-1* and *Δpp-1* mutants compared to wild-type germlings (Figure 1B). We

bioRxiv preprint doi: https://doi.org/10.1101/281931; this version posted March 13, 2018. The copyright holder for this preprint (which was not certified by peer review) is the author/funder, who has granted bioRxiv a license to display the preprint in perpetuity. It is made available under aCC-BY-NC-ND 4.0 International license.

358 defined significant differential expression in each mutant compared to wild-type as -
359 2>$\log_2$FoldChange>2, adjusted p-value<0.01, and consensus among three different
360 programs that calculate differential expression; DESeq2, EdgeR, and Cuffdiff (Files S1
361 and S2).
362
363 We did not identify any significantly up regulated genes in the *Δadv-1* mutant as
364 compared to wild-type germlings; 17 genes were up regulated in *Δpp-1* cells as compared
365 to wild-type germlings (File S1). The *a*-pheromone precursor gene, *mfa-1*, was the most
366 highly expressed gene in *Δpp-1* (*mat a*) germlings (File S1); it is a clear outlier in the top
367 right corner of Figure 1B. These data complement a previous study that used qRT-PCR
368 to show that both *ccg-4* (*A*-pheromone precursor) and *mfa-1* are substantially over-
369 expressed in *Δpp-1* cells as compared to wild-type (Leeder *et al.* 2013), indicating that PP-1
370 specifically represses expression of the mating pheromones in germlings.
371
372 Analyses of RNAseq data identified 155 significantly down regulated genes in either *Δadv-*
373 *1* or *Δpp-1* as compared to wild-type germlings (Figure 2 and File S2). There was
374 substantial overlap between the down regulated genes in both mutants (Figure 1C). Of
375 the down regulated genes in *Δpp-1* germlings, 75% (87/116) were also down regulated in
376 *Δadv-1* cells, while 69% (87/126) of the genes down regulated in *Δadv-1* germlings were
377 also down regulated in *Δpp-1* cells. Before imposing a threshold of significant differential
378 expression, we first calculated the distance between samples on our entire RNAseq
379 dataset. These data further demonstrated that gene expression was more similar between
380 *Δadv-1* and *Δpp-1* germlings than either mutant compared to wild-type germlings (Figure

bioRxiv preprint doi: https://doi.org/10.1101/281931; this version posted March 13, 2018. The copyright holder for this preprint (which was not certified by peer review) is the author/funder, who has granted bioRxiv a license to display the preprint in perpetuity. It is made available under aCC-BY-NC-ND 4.0 International license.

S1). We also did not observe any pattern in the genomic location of genes that are regulated by ADV-1 and/or PP-1 (Figure S2).

In an independent study, expression patterns in the hyphal stage of the *Δadv-1* mutant were compared to those in wild-type hyphae, at three different circadian time points (Dekhang *et al.* 2017). We compared this *Δadv-1* hyphal dataset with our *Δadv-1* germling dataset ($-2<\log_2\text{FoldChange}<2$, adjusted p-value<0.01, Cuffdiff); all genes differentially expressed during at least one time point were included. We found only a modest overlap (26.5%, 39/147) between our *Δadv-1* germling dataset and the *Δadv-1* hyphal dataset (Figure 1D). Of the 39 genes regulated by ADV-1 in both hyphae and germlings (Table S1), 22 are either predicted or known to be involved in the processes of communication, cell fusion, development, or metabolism including *ham-6*, *ham-8*, *ham-11*, *doc-2*, *lfd-1*, *prm-1*, *mat A-1,* and *esd-C* (Glass *et al.* 1988; Han *et al.* 2008; Fleissner *et al.* 2008; Fu *et al.* 2011; Leeder *et al.* 2013; Palma-Guerrero *et al.* 2014; Heller *et al.* 2016). The remaining 19 genes encode hypothetical proteins. Although the overlap between *Δadv-1* RNAseq datasets can be explained by the fact that chemotropic growth and fusion occur during both germling and hyphal stages, there are additional developmental and morphological differences between germlings and hyphae that could explain reduced overlap between the germling and hyphal *Δadv-1* datasets. Consistent with this hypothesis was the observation that our *Δpp-1* germling dataset overlapped with data from a previous single RNAseq experiment on *Δpp-1* germlings (Leeder *et al.* 2013).

Identification of ADV-1 and PP-1 binding sites by DAP-seq

bioRxiv preprint doi: https://doi.org/10.1101/281931; this version posted March 13, 2018. The copyright holder for this preprint (which was not certified by peer review) is the author/funder, who has granted bioRxiv a license to display the preprint in perpetuity. It is made available under aCC-BY-NC-ND 4.0 International license.

DNA-Affinity Purification sequencing (DAP-seq) was recently developed as a high-throughput *in vitro* method for identifying transcription factor binding sites using genomic DNA (O'Malley *et al.* 2016). We adapted this method for *N. crassa*. Briefly, we amplified the *adv-1* and *pp-1* ORFs from cDNA and added a N-terminal HALO-tag to each gene (see Materials and Methods). The HALO-ADV-1 and HALO-PP-1 *in vitro*-synthesized proteins were used for immunoprecipitation experiments using sheared *N. crassa* gDNA that contained adaptors for sequencing. From DAP-seq, we identified PP-1 binding sites that were significantly enriched 2kb upstream of the predicted ATG translation start site for 1953 genes, and ADV-1 binding sites that were significantly enriched within 2kb upstream of the ATG site for 2059 genes ($p<0.0001$, MACS2)(Figure 3A, File S3).

All *in vitro* assays, such as DAP-seq, contain false positives and false negatives because biologically relevant factors are excluded from the assay. For example, a false negative could arise if a transcription factor requires a co-factor to bind a particular sequence of DNA. A false positive could occur if a factor normally blocks a transcription factor from binding a particular DNA sequence. It is also impossible to know from DAP-seq how environmental or biological conditions affect transcription factor binding. In contrast, *in vivo* methods such as ChIPseq provide a snapshot of where a transcription factor binds under the precise environmental and biological conditions of the assay. Comparing data from both DAP-seq and ChIPseq experiments eliminates some of the error associated with each assay. Additional comparison with expression datasets such as RNAseq can elucidate true-positive peaks associated with genes that are directly bound and regulated by a transcription factor.

bioRxiv preprint doi: https://doi.org/10.1101/281931; this version posted March 13, 2018. The copyright holder for this preprint (which was not certified by peer review) is the author/funder, who has granted bioRxiv a license to display the preprint in perpetuity. It is made available under aCC-BY-NC-ND 4.0 International license.

Of the 2059 genes bound by ADV-1 identified with DAP-seq, 273 genes were in consensus with a previous ADV-1 ChIPseq dataset (Dekhang *et al.* 2017). Furthermore, 44 of these 273 genes were differentially expressed in *Δadv-1* germlings versus wild type germlings (Figure 2A). The ADV-1 germling regulon (126 genes)(Figure 2) was enriched for ADV-1 binding sites (consensus between ChIPseq and DAP-seq datasets) as compared to ADV-1 binding sites across the entire genome; 35% of the ADV-1 regulon versus 21% of the genome (p=0.0004, Fisher's Exact Test). Of the 1953 genes bound by PP-1, only 33 genes are differentially expressed in *Δpp-1* vs. wild-type germlings. These 33 genes bound by PP-1 represented 28% of the PP-1 germling regulon (Figure 2), which is what we would expect by chance as compared to the 20% of the entire genome bound by PP-1 (p=0.02, Fisher's Exact Test).

To construct biologically meaningful transcription factor DNA binding motifs, we analyzed only the strongest DAP-seq peaks that were within a 2kb region upstream of differentially expressed genes. These true-positive peaks were enriched for consensus binding motifs (Figure 3B). The ADV-1 binding motif mirrored previously reported ADV-1 binding motifs (Weirauch *et al.* 2014; Dekhang *et al.* 2017). In contrast, our PP-1 motif differed from the PP-1 motif identified using peptide binding arrays (Weirauch *et al.* 2014).

PP-1 and ADV-1 regulate genes required for communication, fusion, growth, and development

bioRxiv preprint doi: https://doi.org/10.1101/281931; this version posted March 13, 2018. The copyright holder for this preprint (which was not certified by peer review) is the author/funder, who has granted bioRxiv a license to display the preprint in perpetuity. It is made available under aCC-BY-NC-ND 4.0 International license.

The *Δadv-1* and *Δpp-1* mutants are impaired in several morphological processes including conidial germination, germling communication, growth rate, aerial hyphae extension, female sexual development, and ascospore germination (Fu *et al.* 2011; Leeder *et al.* 2013; Dekhang *et al.* 2017) (Figure 4, Figure S3, and Table S2). The pleiotropic nature of *Δpp-1* and *Δadv-1* mutants was reflected in the broad functional diversity of the 155 genes that were positively regulated by ADV-1 and/or PP-1 (Figure 2, File S2). These 155 genes fell into three major groups: basic cellular processes (44 genes), communication/fusion/non-self recognition (49 genes), and hypothetical proteins (62 genes). ADV-1 and PP-1 regulate at least some genes in each group, and no group was uniquely regulated by one transcription factor (Figure 2). The significant reduction in growth rate and aerial hyphae in *Δadv-1* and *Δpp-1* cells (Figure 4B,C) can be at least partially explained by the 44 genes whose function was implicated in basic cellular processes such as metabolism, nutrition, growth, development, and general stress response (Figure 2, File S2). Of particular interest to this study are the 49 genes involved in the process of communication, adhesion, fusion, and non-self recognition (Figure 2, File S2). Twenty-two of these 49 genes have been reported previously as being required for normal germling communication, cell fusion, or non-self recognition via heterokaryon incompatibility (Kaneko *et al.* 2006; Kim and Borkovich 2006; Fleissner *et al.* 2008; Fu *et al.* 2011; Leeder *et al.* 2013; Palma-Guerrero *et al.* 2014; Hernández-Galván *et al.* 2015; Lalucque *et al.* 2016; Heller *et al.* 2016, 2018). The remaining 27 genes either have predicted protein domains or homology with proteins implicated in the processes of signaling, adhesion, fusion, cell wall remodeling, or heterokaryon incompatibility.

bioRxiv preprint doi: https://doi.org/10.1101/281931; this version posted March 13, 2018. The copyright holder for this preprint (which was not certified by peer review) is the author/funder, who has granted bioRxiv a license to display the preprint in perpetuity. It is made available under aCC-BY-NC-ND 4.0 International license.

We assessed the germling fusion phenotype for each differentially expressed gene that had an available deletion mutant and that had not previously been described (110 deletion mutants available, 23 mutants not unavailable or heterokaryotic, and 22 mutants previously described). Qualitatively, 106 of these mutants had a wild-type-like germling fusion phenotype. However, four mutants (ΔNCU04645, ΔNCU05836, ΔNCU05916, and ΔNCU04487) had obviously reduced levels of germling fusion. We therefore confirmed that the germling fusion phenotype was due to the deleted gene by co-segregation analysis (data not shown), and we quantified the frequency of germling fusion in each strain (Figure 5A). All four mutants have a significantly reduced frequency of germling fusion compared to the wild-type parental strain ($p<0.01$, ANOVA+TukeyHSD, n=3, ~200-400 germling pairs per sample). ΔNCU04645 was the only mutant that completely lacked any germling communication or fusion. Similarly, ΔNCU04645 was also the only mutant with significantly reduced height of aerial hyphae (Figure 5B, ANOVA+TukeyHSD, $p<0.0001$, n=6)(Figure 5B, S4) and growth rate compared to the wild-type parental strain (Figure 5C, ANOVA+TukeyHSD, $p<0.01$, n=2)(Figure 5C). NCU05836 is predicted to be an ER mannosidase and NCU05916 is a predicted alpha-1,3-mannosyltransferase with homology to the Cu-responsive virulence protein CMT1 in *Cryptococcus neoformans* (Ding *et al.* 2013). Both NCU04487 and NCU04645 are uncharacterized hypothetical proteins. The NCU04487 protein sequence has one predicted C-terminal transmembrane domain and no characterized orthologs. The NCU04645 protein sequence contains a predicted C-terminal AIM24 domain (E-value=1.9E-51, pfam). The AIM24 domain is named after the *S. cerevisiae* protein Aim24p, which is a non-essential mitochondrial inner-membrane protein. In *S. cerevisiae*,

bioRxiv preprint doi: https://doi.org/10.1101/281931; this version posted March 13, 2018. The copyright holder for this preprint (which was not certified by peer review) is the author/funder, who has granted bioRxiv a license to display the preprint in perpetuity. It is made available under aCC-BY-NC-ND 4.0 International license.

496 *Δaim24* mutant shows decreased growth, and Aim24p coordinates the assembly of the
497 MICOS (mitochondrial contact site and cristae organizing system) protein complex
498 (Harner *et al.* 2014).
499
500 Misexpression of *adv-1* suppresses the pleiotropic phenotype of the *Δpp-1* mutant
501 There are four lines of evidence indicating that PP-1 activates transcription of *adv-1,* with
502 ADV-1 as the primary regulator of the PP-1/ADV-1 regulon. First, *adv-1* is down
503 regulated in the *Δpp-1* mutant, but the inverse is not true. Second, our list of 155 ADV-
504 1/PP-1 regulated genes is significantly enriched for ADV-1 binding sites (p=0.0004,
505 Fisher's Exact Test), whereas the same is not true for PP-1 binding sites (p=0.02 Fisher's
506 Exact Test). Third, co-regulated genes are more strongly down regulated in the *Δadv-1*
507 mutant than the *Δpp-1* mutant (Figure 2, File S2). Fourth, there are no potential ADV-1
508 binding motifs upstream of *pp-1,* but there are several potential PP-1 binding motifs
509 upstream of *adv-1*, despite the fact that DAP-seq did not identify PP-1 bound to the *adv-1*
510 promoter. These observations led to the hypothesis that PP-1 regulates *adv-1* and ADV-1
511 directly regulates downstream gene expression.
512
513 To test this hypothesis, we made epitope-tagged misexpression (ME) constructs (*Ptef1-adv-*
514 *1-v5* and *Ptef1-pp-1-v5)* and transformed them into *Δpp-1* and *Δadv-1* cells. Successful
515 misexpression in each mutant was verified by qRT-PCR (Figure 4A). As predicted,
516 expression of *adv-1* was restored in *Δpp-1*(*Ptef1-pp-1-v5)* germlings as compared to the *Δpp-*
517 *1* mutant itself ($p=1.8e^{-7}$, Welch's t-test, n=8). In contrast, expression levels of *pp-1* were
518 equivalent between *Δadv-1*(*Ptef1-adv-1-v5*) and *Δadv-1* germlings (p=0.0045, Welch's t-

bioRxiv preprint doi: https://doi.org/10.1101/281931; this version posted March 13, 2018. The copyright holder for this preprint (which was not certified by peer review) is the author/funder, who has granted bioRxiv a license to display the preprint in perpetuity. It is made available under aCC-BY-NC-ND 4.0 International license.

519 test, n=4) (Figure 4A). Both the *Δadv-1* mutant and the *Δpp-1* mutant have a pleiotropic
520 phenotype when compared with wild-type cells (Figure 4, Figure S3, Table S2). The
521 introduction of *Ptef1-adv-1-v5* fully complemented the pleiotropic phenotype of both *Δadv-*
522 *1* and *Δpp-1* mutants, while the introduction of *Ptef1-pp-1-v5* only complemented the
523 phenotype of the *Δpp-1* mutant, but not the *Δadv-1* mutant (Figure 4 and Figure S3).
524 Collectively, these misexpression experiments support the RNAseq data and the
525 hypothesis that PP-1 controls expression of *adv-1*; ADV-1 is the primary transcriptional
526 regulator of genes involved in cell communication, fusion, protoperithecial development,
527 and growth.
528
529 PP-1 binds the promoter of *adv-1*
530 Given that PP-1 was required for expression of *adv-1*, and misexpression of *adv-1* was
531 sufficient to suppress the phenotype of *Δpp-1* cells, we were surprised that our DAP-seq
532 data failed to identify PP-1 binding to the promoter of *adv-1*. We used the consensus DNA
533 binding motif for each transcription factor (Figure 3B) to search for potential binding sites
534 2kb upstream of both *adv-1* and *pp-1*. Potential ADV-1 binding sites were not identified in
535 the promoter region of either *adv-1* or *pp-1*, however several potential PP-1 binding sites
536 were identified within 2kb of the *adv-1* ORF (Figure 6A). Using antibodies to V5 or GFP,
537 PP-1-bound chromatin was immunoprecipitated from *Δpp-1(Ptef1-pp-1-v5)* and *Δpp-*
538 *1(Pccg1-pp-1-gfp)* germlings. Ten different primer sets in the *adv-1* promoter region were
539 used to interrogate this pool of PP-1-bound DNA. One primer set successfully amplified a
540 region of DNA ~500bp upstream of the *adv-1* ORF (Figure 6B & Figure S5). This
541 immunoprecipitated and amplified region is 127bp long and contains two potential PP-1

bioRxiv preprint doi: https://doi.org/10.1101/281931; this version posted March 13, 2018. The copyright holder for this preprint (which was not certified by peer review) is the author/funder, who has granted bioRxiv a license to display the preprint in perpetuity. It is made available under aCC-BY-NC-ND 4.0 International license.

542 binding sites (Figure 6C). These data confirm our hypothesis that PP-1 binds the
543 promoter and regulates expression of *adv-1*.
544
545 Misexpression of *adv-1* rescues growth defects of *Δmak-1*, but not *Δmak-2* mutants
546 We reasoned that since misexpression (ME) of *adv-1* complemented the phenotype of *Δpp-*
547 *1*, then *MEadv-1* or *MEpp-1* might also complement the phenotype of MAPK mutants
548 predicted to function upstream of these transcription factors. Previous data indicates that
549 the MAK-1 and MAK-2 MAPK pathways engage in crosstalk and likely function
550 upstream of both PP-1 and ADV-1 (Maerz *et al.* 2008; Maddi *et al.* 2012; Dettmann *et al.*
551 2012; Leeder *et al.* 2013; Fu *et al.* 2014). In an effort to elucidate this MAPK-transcription
552 factor network, we misexpressed *adv-1* or *pp-1* in the terminal MAPK mutant (*Δmak-1* and
553 *Δmak-2*) for each MAPK pathway; misexpression was confirmed by qRT-PCR (Figure
554 7A).
555
556 Expression of *adv-1* was effectively zero in *Δmak-1* and *Δmak-2* germlings as compared to
557 wild-type germlings ($p=3.9e^{-19}$ and $p=1.4e^{-23}$ respectively, Welch's t-test, n=8), while
558 expression of *pp-1* was reduced only in *Δmak-2* cells ($p=1.15e^{-9}$, Welch's t-test, n=8)
559 (Figure 7A). These data indicate that MAK-2 functions upstream of both *pp-1* and *adv-1*,
560 while MAK-1 functions upstream of *adv-1* independently of *pp-1*. To test the effect of
561 misexpressing *pp-1* in *Δmak-2* cells, we used a *Δmak-2(Pccg1-pp-1-gfp)* strain; attempts to
562 obtain *Δmak-2(Ptef1-pp-1-v5)* transformants were unsuccessful. The expression of *Pccg1-pp-*
563 *1-gfp* complemented the germling communication, cell fusion, aerial hyphae, and growth
564 rate phenotype of *Δpp-1* cells, but not the sexual defects of the *Δpp-1* mutant (Figure

bioRxiv preprint doi: https://doi.org/10.1101/281931; this version posted March 13, 2018. The copyright holder for this preprint (which was not certified by peer review) is the author/funder, who has granted bioRxiv a license to display the preprint in perpetuity. It is made available under aCC-BY-NC-ND 4.0 International license.

565 S3)(Leeder *et al.* 2013). In contrast to the restoration of *adv-1* expression in *Δpp-1(Ptef1-pp-*
566 *1-v5)* germlings, neither *Δmak-2(Pccg1-pp-1gfp)* nor *Δmak-1(Ptef1-pp-1-v5)* germlings
567 showed increased expression of *adv-1* as compared to *Δmak-2 or Δmak-1* germlings,
568 respectively (p=0.73 and 0.06 respectively, Welch's t-test, n=8). These data indicate that
569 MAK-1 and MAK-2 are necessary for PP-1 dependent transcription of *adv-1*.
570
571 We next assessed the phenotypes of each misexpression mutant. In contrast to *Δpp-*
572 *1(Ptef1-adv-1-v5)*, *Δpp-1(Ptef1-pp-1-v5)*, or *Δpp-1(Pccg1-pp-1-gfp)* cells, misexpression of *Ptef1-*
573 *adv-1-v5* or *Pccg1-pp-1-gfp* did not affect on the phenotype of the *Δmak-2* mutant (Figures
574 7, S3, S6). The misexpression of *Ptef1-pp-1-v5* also had no affect on the phenotype of the
575 *Δmak-1* mutant. However, the misexpression of *Ptef1-adv-1-v5* significantly affected the
576 growth phenotype of the *Δmak-1* mutant (Figure 7B-D). The introduction of *Ptef1-adv-1-v5*
577 into *Δmak-1* cells was sufficient to fully rescue the growth rate defect of the *Δmak-1* mutant
578 (Figure 7C). The *Δmak-1(Ptef1-adv-1-v5)* strain also produced significantly taller aerial
579 hyphae than the *Δmak-1* mutant itself ($p=3.6x10^{-8}$, Welch's t-test, n=6) (Figure 7B), and
580 misexpression of *Ptef1-adv-1-v5* was sufficient to rescue the compact, rosette-like colony
581 morphology of the *Δmak-1* mutant (Figure 7D). However, the introduction of *Ptef1-adv-1-*
582 *v5* was insufficient to rescue the communication and cell fusion defects of the *Δmak-1*
583 mutant (Figure 7E, F), including protoperithecial formation and perithecial development
584 (Figure S6). Together these data indicate that growth defects of the *Δmak-1* mutant can be
585 explained by a simple lack of ADV-1. However, for cell-to-cell communication, cell

bioRxiv preprint doi: https://doi.org/10.1101/281931; this version posted March 13, 2018. The copyright holder for this preprint (which was not certified by peer review) is the author/funder, who has granted bioRxiv a license to display the preprint in perpetuity. It is made available under aCC-BY-NC-ND 4.0 International license.

586 fusion, and sexual reproduction, MAK-1 is clearly necessary, even in the presence of
587 misexpressed *adv-1*.
588
589 *Δpp-1*, *Δmak-2*, and *Δmak-1* cells are sensitive to cell wall stress, and misexpression of *adv-1*
590 or *pp-1* increases resistance in sensitive strains
591 MAK-1 is the terminal MAP kinase in the Cell Wall Integrity (CWI) pathway, which
592 maintains the cell wall during growth and in response to stress (Park *et al.* 2008; Maddi *et*
593 *al.* 2012). Previous studies demonstrated that the *Δmak-1* mutant and other mutants in the
594 CWI pathway are sensitive to the cell wall targeting drugs caspofungin and calcofluor
595 white (Maddi *et al.* 2012). We reasoned that if *Ptef1-adv-1-v5* was sufficient to rescue the
596 growth defects of the *Δmak-1* mutant, then misexpression of *Ptef1-adv-1-v5* might also be
597 sufficient to suppress sensitivity to cell wall stress reagents in *Δmak-1* cells. Additionally,
598 since our data suggested that the MAK-1 and MAK-2 pathways function upstream of
599 both ADV-1 and PP-1, we hypothesized that *Δadv-1*, *Δpp-1*, and *Δmak-2* cells may also be
600 more sensitive to cell wall targeting drugs.
601
602 To test these hypotheses, we assessed growth on agar media containing one of three
603 different cell wall stress drugs; the β-1,3-glucan synthase inhibitor caspofungin (CA), and
604 two different anionic dyes that bind chitin and block chitin-glucan cross-linking;
605 calcofluor white (CFW) and congo red (CR). Wild-type and *Δadv-1* cells were mildly
606 sensitive to all three drugs, while *Δpp-1*, *Δmak-1*, and *Δmak-2* mutants were almost
607 completely unable to grow on all three drugs (Figure 8). Similar to our other growth
608 phenotype data, both the *Δpp-1(Ptef1-pp-1-v5)* and *Δpp-1(Ptef1-adv-1-v5)* strains showed

bioRxiv preprint doi: https://doi.org/10.1101/281931; this version posted March 13, 2018. The copyright holder for this preprint (which was not certified by peer review) is the author/funder, who has granted bioRxiv a license to display the preprint in perpetuity. It is made available under aCC-BY-NC-ND 4.0 International license.

609 wild-type-like resistance to all three drugs. Additionally, the misexpression of *Ptef1-adv-1-*
610 *v5* in *Δmak-1* cells increased its resistance to all three drugs, although this effect was more
611 pronounced on CA than on CFW or CR. The misexpression of *Ptef1-pp-1-v5* in *Δmak-1*
612 cells modestly increased resistance on CFW only. Similarly, the misexpression of *Pccg1-pp-*
613 *1-gfp* in *Δmak-2* cells modestly increased its resistance to all three drugs, while
614 misexpression of *Ptef1-adv-1-v5* in *Δmak-2* cells did not affect resistance. As expected, the
615 introduction of *Ptef1-pp-1-v5* and *Ptef1-pp-1-gfp* into the *Δpp-1* mutant was sufficient to
616 complement the growth defects of the *Δpp-1* mutant on all three drugs (Figure S7). These
617 data indicate that *adv-1* and *pp-1* function downstream of both MAK-2 and MAK-1 to
618 regulate cell-wall stress responsive gene expression.
619

620 **DISCUSSION**

621 Our data supports a model for integrated phosphorylation and transcriptional regulation
622 of genes involved in communication, fusion, growth, development, and cell wall stress
623 response by a network of two MAPK pathways and two transcription factors (Figure 9).
624 The MAK-2 pathway primarily functions upstream of PP-1, while the MAK-1/CWI
625 pathway functions upstream of ADV-1. However, PP-1 also directly regulates
626 transcription of *adv-1,* and there are several points of phosphorylation-mediated cross-talk
627 between the MAK-1 and MAK-2 pathways (Maerz *et al.* 2008; Maddi *et al.* 2012;
628 Dettmann *et al.* 2012, 2013; Leeder *et al.* 2013; Fu *et al.* 2014). Additionally, the catalytic
629 activity of MAK-2 is essential for its function (Leeder *et al.* 2013; Jonkers *et al.* 2014).
630 There are seven MAK-2-dependent phosphorylation sites on PP-1 (Jonkers *et al.* 2014),
631 and the catalytic activity of MAK-2 is required for expression of many PP-1 (and ADV-1)

bioRxiv preprint doi: https://doi.org/10.1101/281931; this version posted March 13, 2018. The copyright holder for this preprint (which was not certified by peer review) is the author/funder, who has granted bioRxiv a license to display the preprint in perpetuity. It is made available under aCC-BY-NC-ND 4.0 International license.

632 regulated genes (Leeder *et al.* 2013). Our qRT-PCR data demonstrated that both MAK-1
633 and MAK-2 were required for PP-1 dependent transcription of *adv-1* (Figure 7A). Our
634 data also indicate that MAK-1 influences *adv-1*-dependent transcription both directly and
635 indirectly via MAK-2 and PP-1. These data combined with the observation that
636 phosphorylation of MAK-2 is reduced in the *Δmak-1* mutant (Maerz *et al.* 2008;
637 Dettmann *et al.* 2012) indicate that MAK-1 is required for full activation of MAK-2, and
638 that MAK-2 is essential for activating or de-repressing PP-1, likely via phosphorylation.
639 Thus, in the absence of fully-activated MAK-2, misexpression of *pp-1* alone is not
640 sufficient to trigger transcription of *adv-1*. Additionally, our observations that MAK-2 is
641 essential for optimal growth rate and resistance to cell wall stress despite misexpression of
642 *pp-1* or *adv-1* (Figures 7,8) suggests that the catalytic activity of MAK-2 may also be
643 important for post-transcriptional regulation of genes important for growth and cell wall
644 stress response.
645
646 The proteins that are dependent on MAK-2 for phosphorylation (either directly or
647 indirectly) are enriched for proteins involved in growth, cell cycle progression,
648 development, signaling, and metabolism (Jonkers *et al.* 2014). There are 40 genes that are
649 both phosphorylated in a MAK-2-dependent manner (Jonkers *et al.* 2014) and regulated
650 by ADV-1 or PP-1 ($1<\log_2 FC<-1$, $p<0.01$, both our data and data from Dekhang *et al.*
651 2017) (Table S3). These 40 genes include the CWI pathway MAPKK *mek-1,* two
652 hypothetical proteins required for germling communication and fusion (*ham-9* and *ham-*
653 *11*), one gene that modulates long-distance non-self recognition (*doc-2*), and several genes
654 broadly involved in growth and metabolism. These genes, in addition to the other
655 communication genes that are regulated by ADV-1 and PP-1 may represent a positive

bioRxiv preprint doi: https://doi.org/10.1101/281931; this version posted March 13, 2018. The copyright holder for this preprint (which was not certified by peer review) is the author/funder, who has granted bioRxiv a license to display the preprint in perpetuity. It is made available under aCC-BY-NC-ND 4.0 International license.

656 feedback loop, in which pathway activation leads to reinforcement. This is particularly
657 true where MEK-1 phosphorylates MAK-1, and then MAK-1 activates transcription of
658 *adv-1*, which in turn activates transcription of MEK-1.
659
660 In addition to the communication and fusion genes, there are three calcium signaling
661 genes that are both phosphorylated by MAK-2 (Jonkers *et al.* 2014) and regulated by
662 ADV-1 and PP-1. These genes, a calcineurin binding protein (NCU01504), a calmodulin-
663 dependent kinase (NCU09212), and a predicted Ca^{2+}/cation channel (NCU08283) are
664 particularly interesting because calcium is required for polarized growth, cell fusion, and
665 stress response (Silverman-Gavrila 2003; Palma-Guerrero *et al.* 2014, 2015; Virgilio *et al.*
666 2017). In other systems, the integration of calcium signaling pathways with MAPK
667 pathways has been well documented. For example, in the dicot plant *Nicotiana benthamiana*,
668 ethylene mediates crosstalk between a hormone responsive MAPK pathway and a
669 calcium-signaling pathway (Ludwig *et al.* 2005).
670
671 Once activated, the CWI and MAK-2 pathways engage in crosstalk that modulates their
672 responses. The signal(s) and receptor(s) involved in germling communication remain
673 elusive, but it is likely that an unidentified receptor leads to activation of the MAK-2
674 pathway. An individual receptor may activate both CWI and MAK-2 pathways, similar
675 to how a receptor-associated-Ras-GTPase activates both the ERK pathway (*mak-2*
676 ortholog) and the PI3K-TORC1 MAPK pathway to regulate cell survival, proliferation,
677 and metabolism in mammalian cells (Mendoza *et al.* 2011). Alternatively, there could be
678 more than one receptor such that some receptors lead to activation of the MAK-2
679 pathway, while other receptors lead to activation of the CWI pathway. The cell wall

bioRxiv preprint doi: https://doi.org/10.1101/281931; this version posted March 13, 2018. The copyright holder for this preprint (which was not certified by peer review) is the author/funder, who has granted bioRxiv a license to display the preprint in perpetuity. It is made available under aCC-BY-NC-ND 4.0 International license.

680 sensors HAM-7 and WSC-1 both function in the CWI pathway and are required for
681 phosphorylation of MAK-1, and to a lesser extent MAK-2 (Maddi *et al.* 2012). However,
682 *ham-7* is essential for germling fusion while *wsc-1* is dispensable, indicating that these two
683 inputs are differentially interpreted through the CWI pathway. The current model
684 suggests that the MAK-2 pathway is primarily activated or repressed by the sensing of
685 extracellular "self" or "non-self" signals, similar to the orthologous pheromone sensing
686 pathway in yeast (Heller *et al.* 2016). Once activated, the MAK-2 pathway works with the
687 CWI pathway to coordinate growth and prepare for cell fusion by regulating expression
688 of genes involved in adhesion, cell wall remodeling, membrane-merging, and post-fusion
689 non-self recognition. Crosstalk reinforces signaling between these pathways when the
690 integrity of the cell wall is maintained and an extracellular "self" signal is present.
691 However, if cell wall integrity is compromised or if extracellular signaling is dampened,
692 then signaling through both the CWI pathway and the MAK-2 is adjusted to confer the
693 correct response to cell wall stress or termination of communication.
694
695 MAP kinases are evolutionarily conserved central regulators for a broad range of cellular
696 processes (Caffrey *et al.* 1999; Xu *et al.* 2016). Crosstalk between MAPK pathways allows
697 for efficient integration of multiple inputs into multiple outputs while also increasing the
698 robustness and plasticity of a signaling network (Jordan *et al.* 2000; Barabási and Oltvai
699 2004; Komarova *et al.* 2005). In *S. cerevisiae*, the CWI pathway and the osmotic stress
700 (HOG) MAPK pathway respond to environmental stress by integrating input from
701 several different cell-surface sensors via cross-activation and downstream crosstalk, which
702 results in a transcriptional response controlled by several different transcription factors
703 (Rodríguez-Peña *et al.* 2010). Flowering plants, such as *A. thaliana* and *Oryza sativa* have

bioRxiv preprint doi: https://doi.org/10.1101/281931; this version posted March 13, 2018. The copyright holder for this preprint (which was not certified by peer review) is the author/funder, who has granted bioRxiv a license to display the preprint in perpetuity. It is made available under aCC-BY-NC-ND 4.0 International license.

704 complex MAPK pathways that are characterized by having several modular MAPKKKs
705 and MAPKs for each individual MAPKK (Chardin *et al.* 2017). There are no clear
706 orthologs to the CWI or MAK-2 pathways in plants, however similar signaling networks
707 exist. For example, in *A. thaliana*, crosstalk between MAPK pathways integrates the
708 response to both abiotic and biotic stresses (Fujita *et al.* 2006).
709
710 In *N. crassa* and closely related *S. macrospora*, the Striatin-Interacting protein Phosphatase
711 and Kinase (STRIPAK) complex regulates MAPK signaling and mediates some crosstalk
712 between the CWI and MAK-2 pathways. The STRIPAK complex localizes to the
713 nuclear envelope, and mutants in the STRIPAK complex have a similar phenotype to
714 mutants in the CWI or MAK-2 pathways (Simonin *et al.* 2010; Bernhards and Pöggeler
715 2011; Fu *et al.* 2011; Dettmann *et al.* 2013; Nordzieke *et al.* 2015; Kück *et al.* 2016; Beier *et*
716 *al.* 2016). Both MAK-1 and MAK-2 have been observed in the nucleus, and the amount
717 of MAK-1 inside the nucleus is dependent on MAK-2 phosphorylating MOB-3, which is
718 a core component of the STRIPAK complex. Furthermore, phosphorylation of MAK-1
719 is reduced in both the *Δmob-3* mutant and another STRIPAK complex mutant, *Δham-3*
720 (Dettmann *et al.* 2012, 2013). Phosphorylated MOB-3 is also broadly required for fruiting
721 body development, but not chemotropic interactions or STRIPAK complex assembly at
722 the nuclear envelope (Dettmann *et al.* 2013). These data illustrate another potential
723 positive feedback loop in which MAK-1 is required for full phosphorylation of MAK-2,
724 and then MAK-2 phosphorylates MOB-3, which is required for both full phosphorylation
725 of MAK-1 and entry of MAK-1 into the nucleus. Furthermore, the STRIPAK complex
726 clearly mediates CWI-MAK-2 pathway cross talk and modulates the output of both
727 pathways. Future experiments will dissect the interconnected signaling network of the

bioRxiv preprint doi: https://doi.org/10.1101/281931; this version posted March 13, 2018. The copyright holder for this preprint (which was not certified by peer review) is the author/funder, who has granted bioRxiv a license to display the preprint in perpetuity. It is made available under aCC-BY-NC-ND 4.0 International license.

728 STRIPAK complex, the CWI pathway, and the MAK-2 pathway. Additionally, further
729 characterization of cell-to-cell communication proteins will reveal novel and potentially
730 conserved features of cell-to-cell communication, cell wall dissolution, and membrane
731 merger across the fungal kingdom.
732
733
734 **DATA AVAILABILITY STATEMENT**
735 DAP-seq raw data is available at the NCBI Sequence Read Archive with accession
736 number (SRP133627). RNAseq raw data (.fastq) is available at the NCBI Sequence Read
737 Archive, accession number SRP133239. Differential expression analysis outputs are
738 included with this publication as File S1. File S2 includes detailed information about the
739 155 differentially expressed genes that we focused on. Results from analyzing DAP-seq
740 data are in File S3.
741
742 **ACKNOWLEDGEMENTS**
743 This work was funded by a grant from the National Science Foundation to NLG
744 (MCB1412411). MSF was supported by NIH Genetics training grant #5T32GM007127-
745 40. VWW was supported by NIH Genetics training grant # 5T32GM007127-39.
746 We acknowledge the use of deletion strains generated by Grant P01 GM068087
747 "Functional Analysis of a Model Filamentous Fungus," which are publicly available at the
748 FGSC. The RNAseq library prep and sequencing was carried out at the DNA
749 Technologies and Expression Analysis Cores at the UC Davis Genome Center, supported
750 by NIH Shared Instrumentation Grant 1S10OD010786-01.
751

bioRxiv preprint doi: https://doi.org/10.1101/281931; this version posted March 13, 2018. The copyright holder for this preprint (which was not certified by peer review) is the author/funder, who has granted bioRxiv a license to display the preprint in perpetuity. It is made available under aCC-BY-NC-ND 4.0 International license.

REFERENCES

Barabási A. L., Oltvai Z. N., 2004 Network biology: understanding the cell's functional organization. Nat. Rev. Genet. 5: 101–113.

Bastiaans E., Debets A. J. M., Aanen D. K., 2015 Experimental demonstration of the benefits of somatic fusion and the consequences for allorecognition. Evolution 69–4: 1091–1099.

Beier A., Teichert I., Krisp C., Wolters D. A., Kück U., 2016 Catalytic Subunit 1 of Protein Phosphatase 2A Is a Subunit of the STRIPAK Complex and Governs Fungal Sexual Development. mBio 7: e00870-16.

Bennett L. D., Beremand P., Thomas T. L., Bell-Pedersen D., 2013 Circadian Activation of the Mitogen-Activated Protein Kinase MAK-1 Facilitates Rhythms in Clock-Controlled Genes in *Neurospora crassa*. Eukaryot. Cell 12: 59–69.

Bernhards Y., Pöggeler S., 2011 The phocein homologue SmMOB3 is essential for vegetative cell fusion and sexual development in the filamentous ascomycete *Sordaria macrospora*. Curr. Genet. 57: 133–149.

Blackwell E., Kim H. J. N., Stone D. E., 2007 The pheromone-induced nuclear accumulation of the Fus3 MAPK in yeast depends on its phosphorylation state and on Dig1 and Dig2. BMC Cell Biol. 8: 44.

Caffrey D. R., O'neill L. A., Shields D. C., 1999 The evolution of the MAP kinase pathways: coduplication of interacting proteins leads to new signaling cascades. J. Mol. Evol. 49: 567–582.

bioRxiv preprint doi: https://doi.org/10.1101/281931; this version posted March 13, 2018. The copyright holder for this preprint (which was not certified by peer review) is the author/funder, who has granted bioRxiv a license to display the preprint in perpetuity. It is made available under aCC-BY-NC-ND 4.0 International license.

773 Chardin C., Schenk S. T., Hirt H., Colcombet J., Krapp A., 2017 Review: Mitogen-
774 Activated Protein Kinases in nutritional signaling in *Arabidopsis*. Plant Sci. 260:
775 101–108.

776 Colot H. V., Park G., Turner G. E., Ringelberg C., Crew C., *et al.*, 2006 A high-
777 throughput gene knockout procedure for *Neurospora* reveals functions for multiple
778 transcription factors. Proc. Natl. Acad. Sci. 103: 13837–13842.

779 Dekhang R., Wu C., Smith K. M., Lamb T. M., Peterson M., *et al.*, 2017 The *Neurospora*
780 Transcription Factor ADV-1 Transduces Light Signals and Temporal
781 Information to Control Rhythmic Expression of Genes Involved in Cell Fusion.
782 Genes|Genomes|Genetics 7: 129–142.

783 Dettmann A., Illgen J., März S., Schürg T., Fleissner A., *et al.*, 2012 The NDR Kinase
784 Scaffold HYM1/MO25 Is Essential for MAK2 MAP Kinase Signaling in
785 *Neurospora crassa*. PLoS Genet. 8: 1–14.

786 Dettmann A., Heilig Y., Ludwig S., Schmitt K., Illgen J., *et al.*, 2013 HAM-2 and HAM-3
787 are central for the assembly of the Neurospora STRIPAK complex at the nuclear
788 envelope and regulate nuclear accumulation of the MAP kinase MAK-1 in a
789 MAK-2-dependent manner. Mol. Microbiol. 90: 796–812.

790 Dettmann A., Heilig Y., Valerius O., Ludwig S., Seiler S., 2014 Fungal Communication
791 Requires the MAK-2 Pathway Elements STE-20 and RAS-2, the NRC-1 Adapter
792 STE-50 and the MAP Kinase Scaffold HAM-5. PLoS Genet. 10: e1004762.

bioRxiv preprint doi: https://doi.org/10.1101/281931; this version posted March 13, 2018. The copyright holder for this preprint (which was not certified by peer review) is the author/funder, who has granted bioRxiv a license to display the preprint in perpetuity. It is made available under aCC-BY-NC-ND 4.0 International license.

793 Ding C., Festa R. A., Chen Y.-L., Espart A., Palacios Ò., *et al.*, 2013 *Cryptococcus neoformans*
794 Copper Detoxification Machinery Is Critical for Fungal Virulence. Cell Host
795 Microbe 13: 265–276.

796 Engh I., Nowrousian M., Kück U., 2010 *Sordaria macrospora*, a model organism to study
797 fungal cellular development. Eur. J. Cell Biol. 89: 864–872.

798 Errede B., Ammerer G., 1989 STE12, a protein involved in cell-type-specific
799 transcription and signal transduction in yeast, is part of protein-DNA complexes.
800 Genes Dev. 3: 1349–1361.

801 Fleissner A., Diamond S., Glass N. L., 2008 The *Saccharomyces cerevisiae* PRM1 Homolog
802 in *Neurospora crassa* Is Involved in Vegetative and Sexual Cell Fusion Events but
803 Also Has Post fertilization Functions. Genetics 181: 497–510.

804 Fleissner A., Leeder A. C., Roca M. G., Read N. D., Glass N. L., 2009 Oscillatory
805 recruitment of signaling proteins to cell tips promotes coordinated behavior
806 during cell fusion. Proc. Natl. Acad. Sci. 106: 19387–19392.

807 Fleissner A., Herzog S., 2016 Signal exchange and integration during self-fusion in
808 filamentous fungi. Semin. Cell Dev. Biol.

809 Freitag M., Hickey P. C., Raju N. B., Selker E. U., Read N. D., 2004 GFP as a tool to
810 analyze the organization, dynamics and function of nuclei and microtubules in
811 *Neurospora crassa*. Fungal Genet. Biol. 41: 897–910.

bioRxiv preprint doi: https://doi.org/10.1101/281931; this version posted March 13, 2018. The copyright holder for this preprint (which was not certified by peer review) is the author/funder, who has granted bioRxiv a license to display the preprint in perpetuity. It is made available under aCC-BY-NC-ND 4.0 International license.

812 Fu C., Iyer P., Herkal A., Abdullah J., Stout A., *et al.*, 2011 Identification and
813 Characterization of Genes Required for Cell-to-Cell Fusion in *Neurospora crassa*.
814 Eukaryot. Cell 10: 1100–1109.

815 Fu C., Ao J., Dettmann A., Seiler S., Free S. J., 2014 Characterization of the *Neurospora*
816 *crassa* Cell Fusion Proteins, HAM-6, HAM-7, HAM-8, HAM-9, HAM-10,
817 AMPH-1 and WHI-2. PLoS ONE 9: e107773.

818 Fujita M., Fujita Y., Noutoshi Y., Takahashi F., Narusaka Y., *et al.*, 2006 Crosstalk
819 between abiotic and biotic stress responses: a current view from the points of
820 convergence in the stress signaling networks. Curr. Opin. Plant Biol. 9: 436–442.

821 Garnjobst L., Wilson J. F., 1952 Heterocaryosis and protoplasmic incompatibility in
822 *Neurospora crassa*. Proc. Natl. Acad. Sci. 42: 613–618.

823 Glass N. L., Vollmer S., Staben C., Grotelueschen J., Metzenberg R. L., *et al.*, 1988
824 DNAs of the two mating-type alleles of Neurospora crassa are highly dissimilar.
825 Science 241: 570–573.

826 Glass N. L., Kaneko I., 2003 Fatal Attraction: Nonself Recognition and Heterokaryon
827 Incompatibility in Filamentous Fungi. Eukaryot. Cell 2: 1–8.

828 Glass N. L., 2004 Hyphal homing, fusion and mycelial interconnectedness. Trends
829 Microbiol. 12: 135–141.

830 Han K.-H., Kim J. H., Moon H., Kim S., Lee S.-S., *et al.*, 2008 The *Aspergillus nidulans*
831 *esdC* (early sexual development) gene is necessary for sexual development and is

bioRxiv preprint doi: https://doi.org/10.1101/281931; this version posted March 13, 2018. The copyright holder for this preprint (which was not certified by peer review) is the author/funder, who has granted bioRxiv a license to display the preprint in perpetuity. It is made available under aCC-BY-NC-ND 4.0 International license.

controlled by *veA* and a heterotrimeric G protein. Fungal Genet. Biol. 45: 310–318.

Harner M. E., Unger A. K., Izawa T., Walther D. M., Özbalci C., *et al.*, 2014 Aim24 and MICOS modulate respiratory function, tafazzin-related cardiolipin modification and mitochondrial architecture. Elife 3:e01684.

Heller J., Zhao J., Rosenfield G., Kowbel D. J., Gladieux P., *et al.*, 2016 Characterization of Greenbeard Genes Involved in Long-Distance Kind Discrimination in a Microbial Eukaryote. PLOS Biol. 14: e1002431.

Heller J., Clavé C., Gladieux P., Saupe S. J., Glass N. L., 2018 NLR surveillance of essential SEC-9 SNARE proteins induces programmed cell death upon allorecognition in filamentous fungi. Proc. Natl. Acad. Sci. Epub ahead of print.

Hernández-Galván M., Cano-Domínguez N., Robledo-Briones A., Castro-Longoria E., Lichius A., *et al.*, 2015 The tetraspanin PLS-1 is required for NOX-1 and NOX-2 functions in cell fusion, cell growth and differentiation in the fungus *Neurospora crassa*. In: *Fungal Genetics Reports*, 61(Suppl). Pacific Grove, CA, p. 66.

Hickey P. C., Jacobson D. J., Read N. D., Glass N. L., 2002 Live-cell imaging of vegetative hyphal fusion in *Neurospora crassa*. Fungal Genet. Biol. 37: 109–119.

Jonkers W., Leeder A. C., Ansong C., Wang Y., Yang F., *et al.*, 2014 HAM-5 Functions As a MAP Kinase Scaffold during Cell Fusion in *Neurospora crassa*. PLoS Genet. 10: e1004783.

bioRxiv preprint doi: https://doi.org/10.1101/281931; this version posted March 13, 2018. The copyright holder for this preprint (which was not certified by peer review) is the author/funder, who has granted bioRxiv a license to display the preprint in perpetuity. It is made available under aCC-BY-NC-ND 4.0 International license.

852 Jordan J. D., Landau E. M., Iyengar R., 2000 Signaling networks: the origins of cellular
853 multitasking. Cell 103: 193–200.

854 Kaneko I., Dementhon K., Xiang Q., Glass N. L., 2006 Nonallelic Interactions Between
855 *het-c* and a Polymorphic Locus, *pin-c*, Are Essential for Nonself Recognition and
856 Programmed Cell Death in *Neurospora crassa*. Genetics 172: 1545–1555.

857 Kim H., Borkovich K. A., 2004 A pheromone receptor gene, *pre-1*, is essential for mating
858 type-specific directional growth and fusion of trichogynes and female fertility in
859 *Neurospora crassa*: Pheromone response pathway in *N. crassa*. Mol. Microbiol. 52:
860 1781–1798.

861 Kim H., Borkovich K. A., 2006 Pheromones Are Essential for Male Fertility and
862 Sufficient To Direct Chemotropic Polarized Growth of Trichogynes during
863 Mating in *Neurospora crassa*. Eukaryot. Cell 5: 544–554.

864 Kim D., Pertea G., Trapnell C., Pimentel H., Kelley R., *et al.*, 2013 TopHat2: accurate
865 alignment of transcriptomes in the presence of insertions, deletions and gene
866 fusions. Genome Biol. 14: R36.

867 Komarova N. L., Zou X., Nie Q., Bardwell L., 2005 A theoretical framework for
868 specificity in cell signaling. Mol. Syst. Biol. 1: E1–E5.

869 Krzywinski M., Schein J., Birol I., Connors J., Gascoyne R., *et al.*, 2009 Circos: an
870 information aesthetic for comparative genomics. Genome Res. 19: 1639–1645.

bioRxiv preprint doi: https://doi.org/10.1101/281931; this version posted March 13, 2018. The copyright holder for this preprint (which was not certified by peer review) is the author/funder, who has granted bioRxiv a license to display the preprint in perpetuity. It is made available under aCC-BY-NC-ND 4.0 International license.

871 Kück U., Beier A. M., Teichert I., 2016 The composition and function of the striatin-
872 interacting phosphatases and kinases (STRIPAK) complex in fungi. Fungal Genet.
873 Biol. 90: 31–38.

874 Lalucque H., Malagnac F., Green K., Gautier V., Grognet P., *et al.*, 2016 IDC2 and
875 IDC3, two genes involved in cell non-autonomous signaling of fruiting body
876 development in the model fungus *Podospora anserina*. Dev. Biol. 421: 126–138.

877 Langmead B., Trapnell C., Pop M., Salzberg S. L., 2009 Ultrafast and memory-efficient
878 alignment of short DNA sequences to the human genome. Genome Biol. 10: R25.

879 Leeder A. C., Jonkers W., Li J., Glass N. L., 2013 Early Colony Establishment in
880 *Neurospora crassa* Requires a MAP Kinase Regulatory Network. Genetics 195: 883–
881 898.

882 Li D., 2005 A Mitogen-Activated Protein Kinase Pathway Essential for Mating and
883 Contributing to Vegetative Growth in *Neurospora crassa*. Genetics 170: 1091–1104.

884 Li H., Handsaker B., Wysoker A., Fennell T., Ruan J., *et al.*, 2009 The Sequence
885 Alignment/Map format and SAMtools. Bioinformatics 25: 2078–2079.

886 Livak K. J., Schmittgen T. D., 2001 Analysis of Relative Gene Expression Data Using
887 Real-Time Quantitative PCR and the $2^{-\Delta\Delta CT}$ Method. Methods 25: 402–408.

888 Love M. I., Huber W., Anders S., 2014 Moderated estimation of fold change and
889 dispersion for RNA-seq data with DESeq2. Genome Biol. 15:550.

bioRxiv preprint doi: https://doi.org/10.1101/281931; this version posted March 13, 2018. The copyright holder for this preprint (which was not certified by peer review) is the author/funder, who has granted bioRxiv a license to display the preprint in perpetuity. It is made available under aCC-BY-NC-ND 4.0 International license.

890 Ludwig A. A., Saitoh H., Felix G., Freymark G., Miersch O., *et al.*, 2005 Ethylene-
891 mediated cross-talk between calcium-dependent protein kinase and MAPK
892 signaling controls stress responses in plants. Proc. Natl. Acad. Sci. U. S. A. 102:
893 10736–10741.

894 Maddi A., Dettman A., Fu C., Seiler S., Free S. J., 2012 WSC-1 and HAM-7 Are MAK-
895 1 MAP Kinase Pathway Sensors Required for Cell Wall Integrity and Hyphal
896 Fusion in *Neurospora crassa*. PLoS ONE 7: e42374.

897 Maerz S., Ziv C., Vogt N., Helmstaedt K., Cohen N., *et al.*, 2008 The Nuclear Dbf2-
898 Related Kinase COT1 and the Mitogen-Activated Protein Kinases MAK1 and
899 MAK2 Genetically Interact to Regulate Filamentous Growth, Hyphal Fusion and
900 Sexual Development in *Neurospora crassa.* Genetics 179: 1313–1325.

901 Masloff S., Pöggeler S., Kück U., 1999 The *pro1*+ gene from *Sordaria macrospora* encodes a
902 C6 zinc finger transcription factor required for fruiting body development.
903 Genetics 152: 191–199.

904 Masloff S., Jacobsen S., Pöggeler S., Kück U., 2002 Functional analysis of the C_6 zinc
905 finger gene *pro1* involved in fungal sexual development. Fungal Genet. Biol. 36:
906 107–116.

907 McCarthy D. J., Chen Y., Smyth G. K., 2012 Differential expression analysis of
908 multifactor RNA-Seq experiments with respect to biological variation. Nucleic
909 Acids Res. 40: 4288–4297.

bioRxiv preprint doi: https://doi.org/10.1101/281931; this version posted March 13, 2018. The copyright holder for this preprint (which was not certified by peer review) is the author/funder, who has granted bioRxiv a license to display the preprint in perpetuity. It is made available under aCC-BY-NC-ND 4.0 International license.

910 Mendoza M. C., Er E. E., Blenis J., 2011 The Ras-ERK and PI3K-mTOR pathways:
911 cross-talk and compensation. Trends Biochem. Sci. 36: 320–328.

912 Merlini L., Dudin O., Martin S. G., 2013 Mate and fuse: how yeast cells do it. Open Biol.
913 3: 130008–130008.

914 Nordzieke S., Zobel T., Fränzel B., Wolters D. A., Kück U., *et al.*, 2015 A Fungal
915 Sarcolemmal Membrane-Associated Protein (SLMAP) Homolog Plays a
916 Fundamental Role in Development and Localizes to the Nuclear Envelope,
917 Endoplasmic Reticulum, and Mitochondria. Eukaryot. Cell 14: 345–358.

918 Nowrousian M., Frank S., Koers S., Strauch P., Weitner T., *et al.*, 2007 The novel ER
919 membrane protein PRO41 is essential for sexual development in the filamentous
920 fungus *Sordaria macrospora*. Mol. Microbiol. 64: 923–937.

921 O'Malley R. C., Huang S. C., Song L., Lewsey M. G., Bartlett A., *et al.*, 2016 Cistrome
922 and Epicistrome Features Shape the Regulatory DNA Landscape. Cell 165:
923 1280–1292.

924 Palma-Guerrero J., Hall C. R., Kowbel D., Welch J., Taylor J. W., *et al.*, 2013 Genome
925 Wide Association Identifies Novel Loci Involved in Fungal Communication. PLoS
926 Genet. 9: 1–13.

927 Palma-Guerrero J., Leeder A. C., Welch J., Glass N. L., 2014 Identification and
928 characterization of LFD1, a novel protein involved in membrane merger during
929 cell fusion in *Neurospora crassa*. Mol. Microbiol. 92: 164–182.

bioRxiv preprint doi: https://doi.org/10.1101/281931; this version posted March 13, 2018. The copyright holder for this preprint (which was not certified by peer review) is the author/funder, who has granted bioRxiv a license to display the preprint in perpetuity. It is made available under aCC-BY-NC-ND 4.0 International license.

930 Palma-Guerrero J., Zhao J., Gonçalves A. P., Starr T. L., Glass N. L., 2015 Identification
931 and Characterization of LFD-2, a Predicted Fringe Protein Required for
932 Membrane Integrity during Cell Fusion in *Neurospora crassa*. Eukaryot. Cell 14:
933 265–277.

934 Pandit A., Maheshwari R., 1994 A simple method of obtaining pure microconidia in
935 *Neurospora crassa*. Fungal Genet. Newsl. 41: 64–65.

936 Park G., Pan S., Borkovich K. A., 2008 Mitogen-Activated Protein Kinase Cascade
937 Required for Regulation of Development and Secondary Metabolism in *Neurospora*
938 *crassa*. Eukaryot. Cell 7: 2113–2122.

939 Perbal B., 2003 Communication is the key. Cell Commun. Signal. 1: 3.

940 Read N. D., Goryachev A. B., Lichius A., 2012 The mechanistic basis of self-fusion
941 between conidial anastomosis tubes during fungal colony initiation. Fungal Biol.
942 Rev. 26: 1–11.

943 Richard F., Glass N. L., Pringle A., 2012 Cooperation among germinating spores
944 facilitates the growth of the fungus, *Neurospora crassa*. Biol. Lett. 8: 419–422.

945 Roberts A., Trapnell C., Donaghey J., 2010 Improving RNA-Seq expression estimates by
946 correcting for fragment bias.

947 Robinson M. D., McCarthy D. J., Smyth G. K., 2010 edgeR: a Bioconductor package for
948 differential expression analysis of digital gene expression data. Bioinformatics 26:
949 139–140.

bioRxiv preprint doi: https://doi.org/10.1101/281931; this version posted March 13, 2018. The copyright holder for this preprint (which was not certified by peer review) is the author/funder, who has granted bioRxiv a license to display the preprint in perpetuity. It is made available under aCC-BY-NC-ND 4.0 International license.

950 Rodríguez-Peña J. M., García R., Nombela C., Arroyo J., 2010 The high-osmolarity
951 glycerol (HOG) and cell wall integrity (CWI) signalling pathways interplay: a yeast
952 dialogue between MAPK routes. Yeast 27: 495–502.

953 Saupe S. J., 2000 Molecular genetics of heterokaryon incompatibility in filamentous
954 ascomycetes. Microbiol. Mol. Biol. Rev. 64: 489–502.

955 Silverman-Gavrila L. B., 2003 Calcium gradient dependence of *Neurospora crassa* hyphal
956 growth. Microbiology 149: 2475–2485.

957 Simonin A. R., Rasmussen C. G., Yang M., Glass N. L., 2010 Genes encoding a striatin-
958 like protein (*ham-3*) and a forkhead associated protein (*ham-4*) are required for
959 hyphal fusion in *Neurospora crassa*. Fungal Genet. Biol. 47: 855–868.

960 Simonin A., Palma-Guerrero J., Fricker M., Glass N. L., 2012 Physiological Significance
961 of Network Organization in Fungi. Eukaryot. Cell 11: 1345–1352.

962 Smith K. M., Sancar G., Dekhang R., Sullivan C. M., Li S., *et al.*, 2010 Transcription
963 Factors in Light and Circadian Clock Signaling Networks Revealed by
964 Genomewide Mapping of Direct Targets for *Neurospora* White Collar Complex.
965 Eukaryot. Cell 9: 1549–1556.

966 Teichert I., Steffens E. K., Schnaß N., Fränzel B., Krisp C., *et al.*, 2014 PRO40 Is a
967 Scaffold Protein of the Cell Wall Integrity Pathway, Linking the MAP Kinase
968 Module to the Upstream Activator Protein Kinase C. PLoS Genet. 10: e1004582.

969 Virgilio S., Cupertino F. B., Ambrosio D. L., Bertolini M. C., 2017 Regulation of the
970 reserve carbohydrate metabolism by alkaline pH and calcium in *Neurospora crassa*

bioRxiv preprint doi: https://doi.org/10.1101/281931; this version posted March 13, 2018. The copyright holder for this preprint (which was not certified by peer review) is the author/funder, who has granted bioRxiv a license to display the preprint in perpetuity. It is made available under aCC-BY-NC-ND 4.0 International license.

reveals a possible cross-regulation of both signaling pathways. BMC Genomics 18:457.

Vogel H. J., 1956 A convenient growth medium for Neurospora (Medium N). Microb. Genet. Bull.: 42–43.

Weichert M., Lichius A., Priegnitz B.-E., Brandt U., Gottschalk J., *et al.*, 2016 Accumulation of specific sterol precursors targets a MAP kinase cascade mediating cell–cell recognition and fusion. Proc. Natl. Acad. Sci. 113(42):11877-11882.

Weirauch M. T., Yang A., Albu M., Cote A. G., Montenegro-Montero A., *et al.*, 2014 Determination and Inference of Eukaryotic Transcription Factor Sequence Specificity. Cell 158: 1431–1443.

Westergaard M., Mitchell H. K., 1947 *Neurospora* V. A Synthetic Medium Favoring Sexual Reproduction. Am. J. Bot. 34: 573.

Xiong Y., Coradetti S. T., Li X., Gritsenko M. A., Clauss T., *et al.*, 2014 The proteome and phosphoproteome of *Neurospora crassa* in response to cellulose, sucrose and carbon starvation. Fungal Genet. Biol. 72: 21–33.

Xu C., Liu R., Zhang Q., Chen X., Qian Y., *et al.*, 2016 The diversification of evolutionarily conserved MAPK cascades correlates with the evolution of fungal species and development of lifestyles. Genome Biol. Evol.: evw051.

Zhang Y., Liu T., Meyer C. A., Eeckhoute J., Johnson D. S., *et al.*, 2008 Model-based Analysis of ChIP-Seq (MACS). Genome Biol. 9: R137.

bioRxiv preprint doi: https://doi.org/10.1101/281931; this version posted March 13, 2018. The copyright holder for this preprint (which was not certified by peer review) is the author/funder, who has granted bioRxiv a license to display the preprint in perpetuity. It is made available under aCC-BY-NC-ND 4.0 International license.

992

bioRxiv preprint doi: https://doi.org/10.1101/281931; this version posted March 13, 2018. The copyright holder for this preprint (which was not certified by peer review) is the author/funder, who has granted bioRxiv a license to display the preprint in perpetuity. It is made available under aCC-BY-NC-ND 4.0 International license.

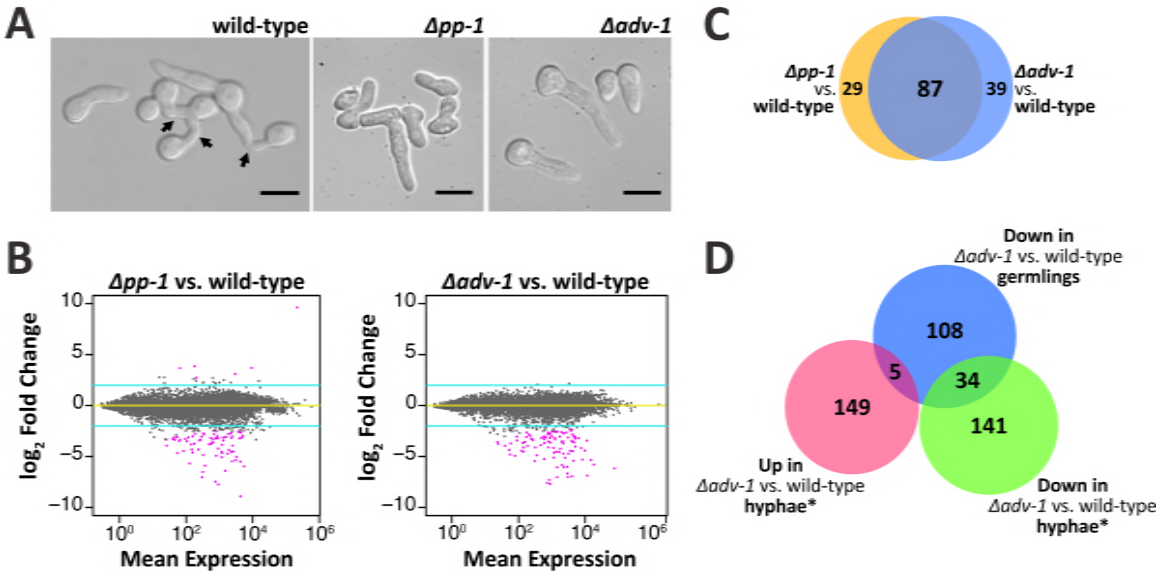

Figure 1. ADV-1 and PP-1 have a shared regulon in germlings.

(A) Microscopic images showing germling morphology at the time point when we extracted RNA for RNAseq. Arrows indicate fusion events. **(B)** MA plots depicting total RNAseq data for each transcription factor mutant versus the parental wild-type strain. Turquoise lines denote threshold of $2<\log_2 FC<-2$, and pink points indicate genes with significant differential expression ($p<0.01$, DESeq2). **(C)** Number of genes significantly down regulated in each mutant as compared to the wild-type parental strain (consensus between CuffDiff, EdgeR, and DESeq2, $\log_2 FC<-2$ and adjusted p-value<0.01). Blue circle is *Δadv-1* compared to wild-type germlings, orange circle is *Δpp-1* compared to wild-type germlings. **(D)** Number of significantly differentially expressed genes in *Δadv-1 as* compared to the parental wild-type strain in hyphae* compared to germlings ($-2>\log_2 FC>2$ and $p<0.01$, Cuffdiff). *Hyphal data from Dekhang *et al.* 2017 where RNAseq data was collected from three different time points. Genes were included if they were differentially expressed during at least one time point.

bioRxiv preprint doi: https://doi.org/10.1101/281931; this version posted March 13, 2018. The copyright holder for this preprint (which was not certified by peer review) is the author/funder, who has granted bioRxiv a license to display the preprint in perpetuity. It is made available under aCC-BY-NC-ND 4.0 International license.

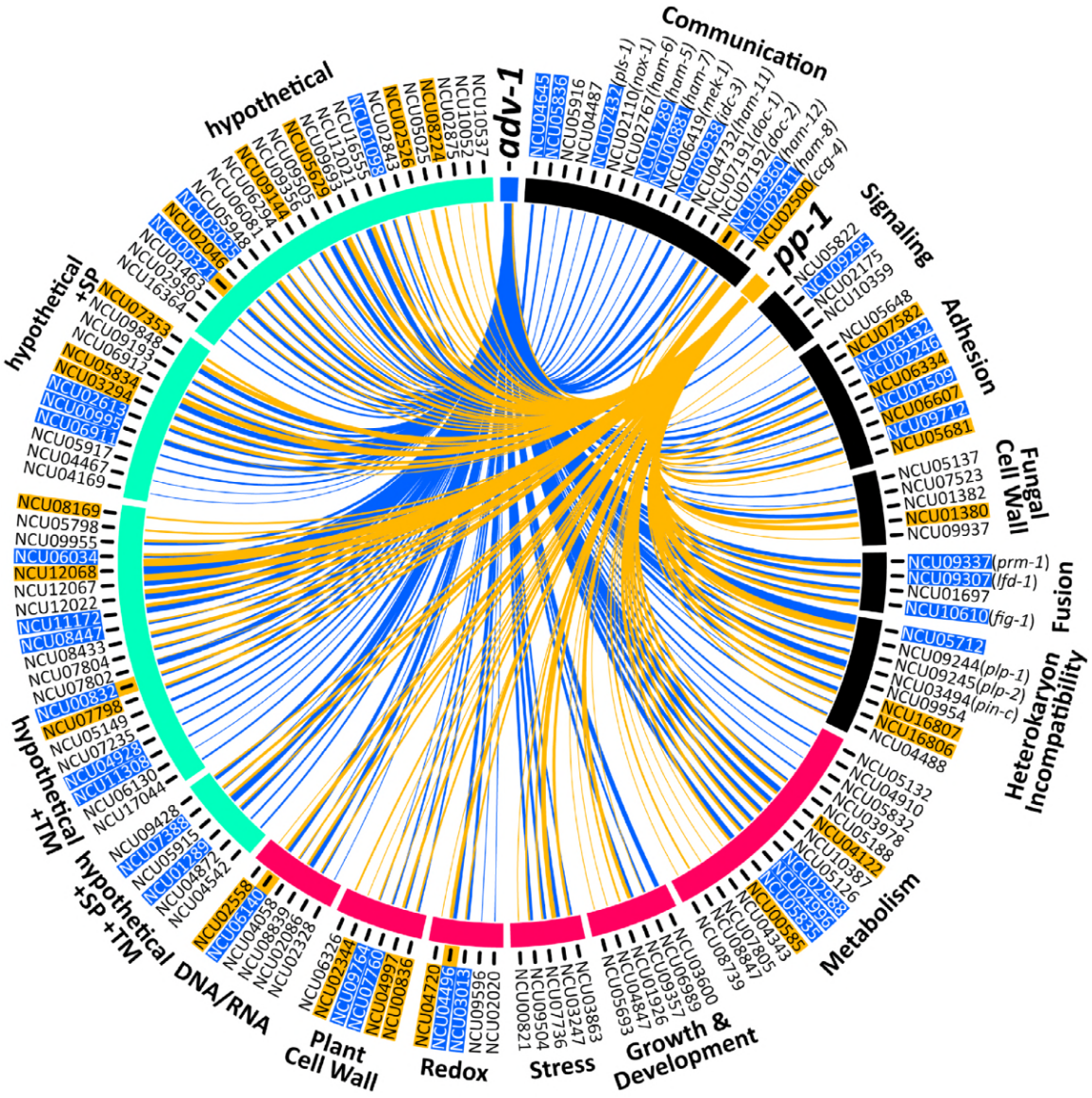

1009

1010 **Figure 2. Genes that are positively regulated by ADV-1 and PP-1 in**

1011 **germlings**. Circos plots depicting the 155 genes that are significantly down regulated in

1012 either *Δadv-1* or *Δpp-1* germlings as compared to parental wild-type germlings ($log_2FC<-2$

1013 and $p<0.01$, consensus among Cuffdiff, DESeq2, and EdgeR). Genes are organized based

1014 on function that is either known from previous work, or inferred via homology and

1015 protein prediction. Gene function is clustered into three major groups: communication

1016 and fusion (black), basic cellular processes (magenta), and hypothetical proteins (seafoam

bioRxiv preprint doi: https://doi.org/10.1101/281931; this version posted March 13, 2018. The copyright holder for this preprint (which was not certified by peer review) is the author/funder, who has granted bioRxiv a license to display the preprint in perpetuity. It is made available under aCC-BY-NC-ND 4.0 International license.

1017 green). Blue lines indicate genes that are regulated by ADV-1, orange lines indicate genes
1018 that are regulated by PP-1, and line thickness is proportional to the fold-change difference
1019 in expression between the transcription factor mutant and wild type germlings. Gene IDs
1020 are highlighted to indicate the presence of at least one ADV-1 (blue) or PP-1 (orange)
1021 binding site in the promoter region within 2kb upstream of ATG. Five genes were bound
1022 by both ADV-1 and PP-1; these gene IDs are highlighted with blue and have an
1023 additional orange highlight immediately adjacent to the gene ID. PP-1 binding sites were
1024 determined by consensus between DAPseq and RNAseq, and ADV-1 binding sites are
1025 the consensus between DAPseq, RNAseq, and ChIPseq datasets. ChIPseq data is
1026 available from Dekhang *et al.* 2017, in which ChIPseq was performed at three different
1027 time points. Genes were included here if they were bound by ADV-1 during at least one
1028 time point. This list of 155 genes is significantly enriched for ADV-1 binding sites
1029 ($p=0.0004$, Fisher's Exact Test), but not PP-1 binding sites ($p=0.02$, Fisher's Exact Test).
1030

bioRxiv preprint doi: https://doi.org/10.1101/281931; this version posted March 13, 2018. The copyright holder for this preprint (which was not certified by peer review) is the author/funder, who has granted bioRxiv a license to display the preprint in perpetuity. It is made available under aCC-BY-NC-ND 4.0 International license.

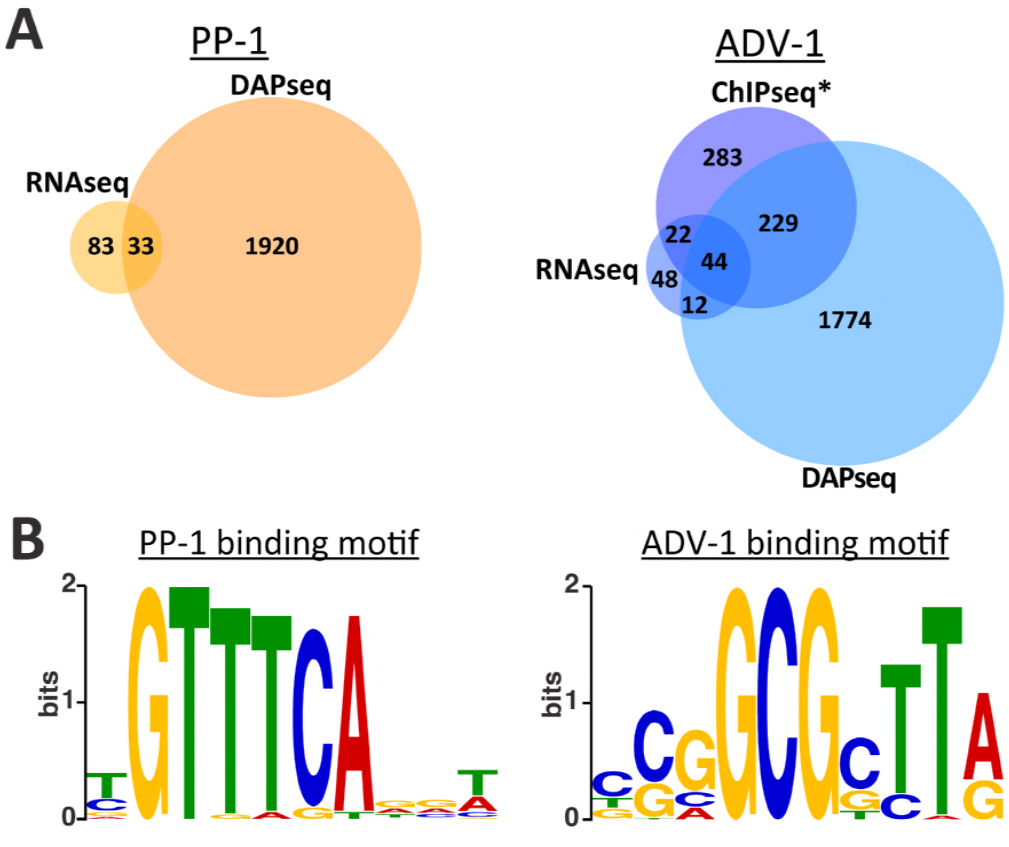

1031

1032 **Figure 3. DAPseq identifies promoters bound by ADV-1 or PP-1.**

1033 **(A)** Number of genes that are down regulated in *Δpp-1* germlings (RNAseq) or bound by

1034 PP-1 (DAPseq) (left panel). The number of genes that are down regulated in *Δadv-1*

1035 germlings (RNAseq) or bound by ADV-1 (DAPseq and ChIPseq) (right panel). Down

1036 regulated genes were identified by consensus between CuffDiff, EdgeR, and DESeq2,

1037 $\log_2$FC<-2 and adjusted p-value<0.01 (compare with Figure 1C). Genes bound by each

1038 transcription factor were counted if the transcription factor was bound within 2kb

1039 upstream of the ATG (p<0.001). *ADV-1 ChIPseq data is available from Dekhang *et al.*

1040 2017, in which ChIPseq was performed at three different time points. Genes were

1041 included here if they were bound by ADV-1 during at least one time point. **(B)**

1042 Consensus DNA binding motif for PP-1 or ADV-1 based on DAPseq data.

1043

bioRxiv preprint doi: https://doi.org/10.1101/281931; this version posted March 13, 2018. The copyright holder for this preprint (which was not certified by peer review) is the author/funder, who has granted bioRxiv a license to display the preprint in perpetuity. It is made available under aCC-BY-NC-ND 4.0 International license.

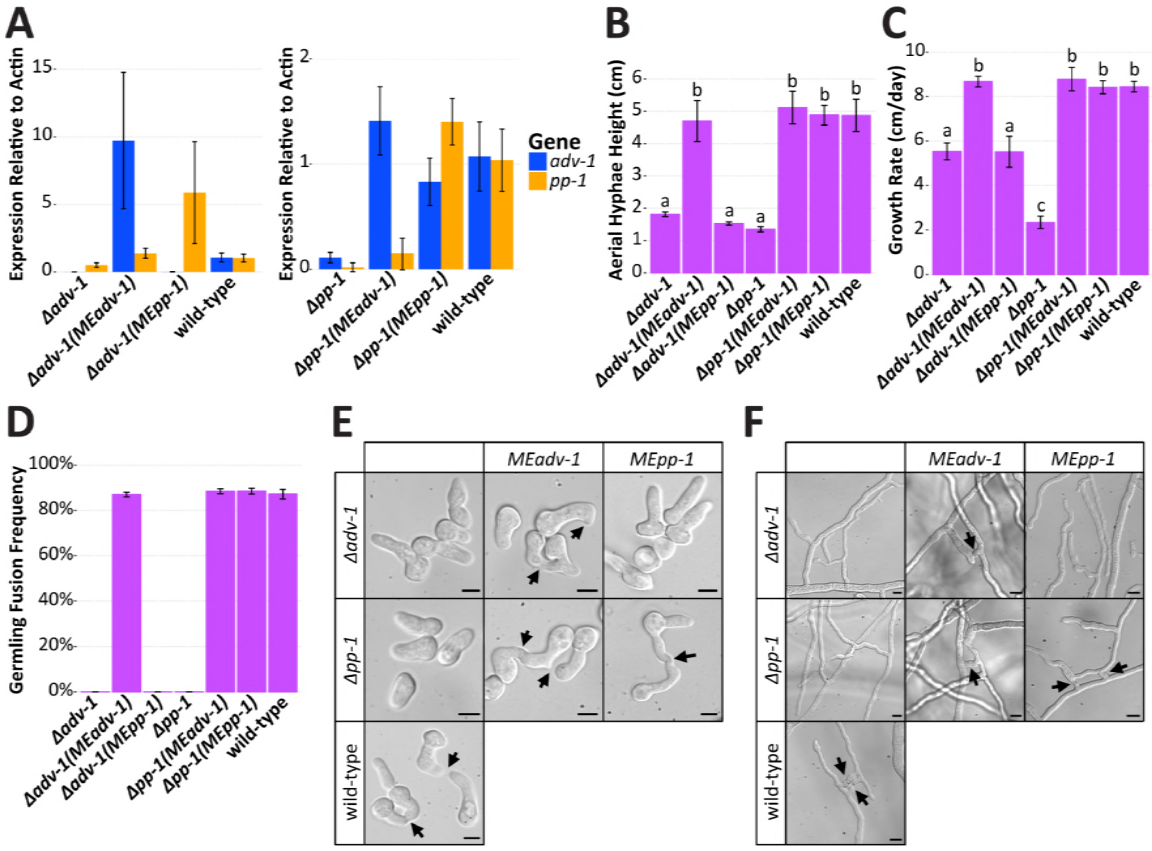

Figure 4. Misexpression of *adv-1* suppresses the phenotype of the *Δpp-1* mutant. (A) qRT-PCR data showing mRNA expression levels of *adv-1* and *pp-1* in *Δadv-1 (Ptef1-adv-1-v5; his-3* (*MEadv-1*)) and *Δadv-1 (Ptef1-pp-1-v5; his-3* (*MEpp-1*)) germlings (left panel) and in *Δpp-1* (*Ptef1-adv-1-v5; his-3* (*MEadv-1*)) and *Δpp-1 (Ptef1-pp1-v5;his-3* (*MEpp-1*)) germlings (right panel) compared to the wild type parental strain. **(B)** Mean height of aerial hyphae of strains in (A) three days after inoculation (ANOVA+TukeyHSD, $p<0.0001$, n=6). **(C)** Mean growth rate per 24 hrs of strains in (A) measured over 4 days (ANOVA+TukeyHSD, $p<0.01$, n=3). **(D)** Mean frequency of communication and fusion between pairs of germlings for each strain in (A) (n=3, 400-700 germling pairs counted per sample). For all bar plots, error bars indicate standard deviation. **(E)** Photos of the germlings (scale bars = 5μm) and **(F)** hyphae (scale bars = 10μm) for each strain in (A).

bioRxiv preprint doi: https://doi.org/10.1101/281931; this version posted March 13, 2018. The copyright holder for this preprint (which was not certified by peer review) is the author/funder, who has granted bioRxiv a license to display the preprint in perpetuity. It is made available under aCC-BY-NC-ND 4.0 International license.

Arrows indicate chemotropic interactions and successful cell fusion.

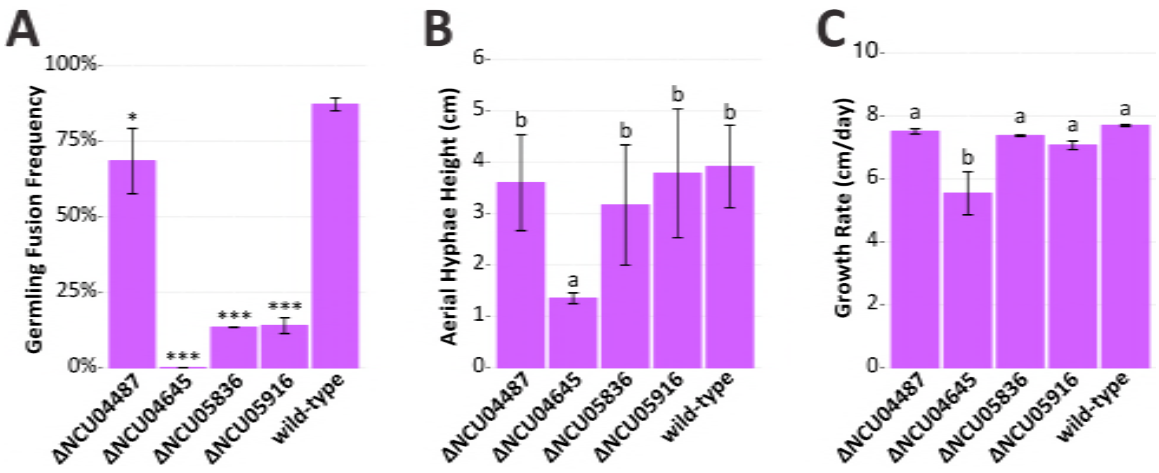

Figure 5. Four ADV-1-regulated genes are required for normal germling fusion and growth.

A screen of 110 deletion mutants of the 155 genes regulated by ADV-1 and/or PP-1 revealed that strains carrying mutations in four genes have cell fusion defects. The remaining 151 mutants either have a previously described germling fusion defect, wild-type like germling fusion phenotype, or homokaryotic deletion mutants are not available in the deletion collection. **(A)** ΔNCU04487, ΔNCU04645, ΔNCU05836 and ΔNCU05916 mutants showed reduced germling fusion. Mean germling fusion frequency of each mutant and wild type (n=3, ~200-400 germling pairs counted per sample). Stars indicate a significant difference compared to the parental wild type strain (*p=0.007, ***p<1E-7, ANOVA+TukeyHSD). **(B)** Mean height of aerial hyphae of ΔNCU04487, ΔNCU04645, ΔNCU05836 and ΔNCU05916 mutants three days after inoculation (ANOVA+TukeyHSD, p<0.0001, n=6). **(C)** Mean growth rate of ΔNCU04487, ΔNCU04645, ΔNCU05836 and ΔNCU05916 mutants per day measured over 4 days (ANOVA+TukeyHSD, p<0.01, n=2). For all bar plots, error bars indicate standard

bioRxiv preprint doi: https://doi.org/10.1101/281931; this version posted March 13, 2018. The copyright holder for this preprint (which was not certified by peer review) is the author/funder, who has granted bioRxiv a license to display the preprint in perpetuity. It is made available under aCC-BY-NC-ND 4.0 International license.

1074 deviation.

1075

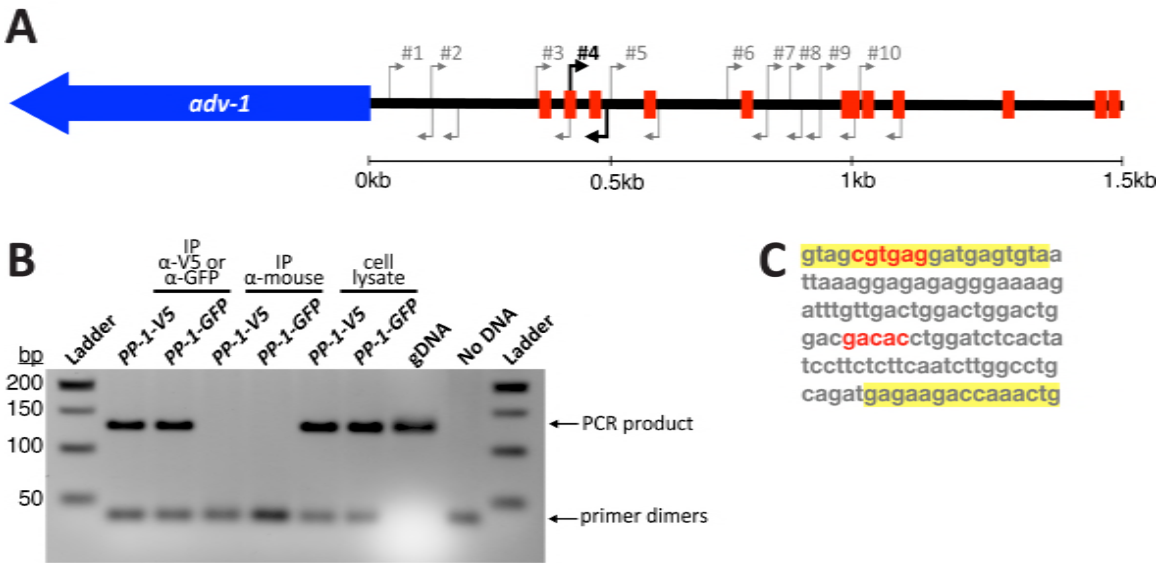

1076

1077 **Figure 6. ChIP-PCR identifies a PP-1 binding site ~500bp upstream of the**

1078 ***adv-1* ORF.**

1079 **(A)** Diagram of predicted PP-1 binding sites within 1.5kb upstream of *adv-1* ORF, based

1080 on the motif depicted in Figure 2B. Arrows indicate ten different PCR primer sets used to

1081 interrogate immunoprecipitated chromatin. **(B)** Agarose DNA gel showing results of

1082 ChIP-PCR with primer set #4. The remaining PCR results are included in Figure S5.

1083 Immunoprecipitation with *Δpp-1(Ptef1-pp-1-v5; his-3)* and *Δpp-1(Pccg1-pp-1-gfp; his-3)*

1084 strains was performed using α-V5 or α-GFP antibodies. α-mouse antibodies were used as

1085 a negative control. Whole cell lysate and independent *N. crassa* genomic DNA were

1086 included as positive PCR controls, with a PCR reaction lacking DNA as an additional

1087 negative control. **(C)** The sequence of the PCR product in (B). Primers highlighted with

1088 yellow correspond to primer set #4 in (A), predicted PP-1 binding sites are in red.

1089

bioRxiv preprint doi: https://doi.org/10.1101/281931; this version posted March 13, 2018. The copyright holder for this preprint (which was not certified by peer review) is the author/funder, who has granted bioRxiv a license to display the preprint in perpetuity. It is made available under aCC-BY-NC-ND 4.0 International license.

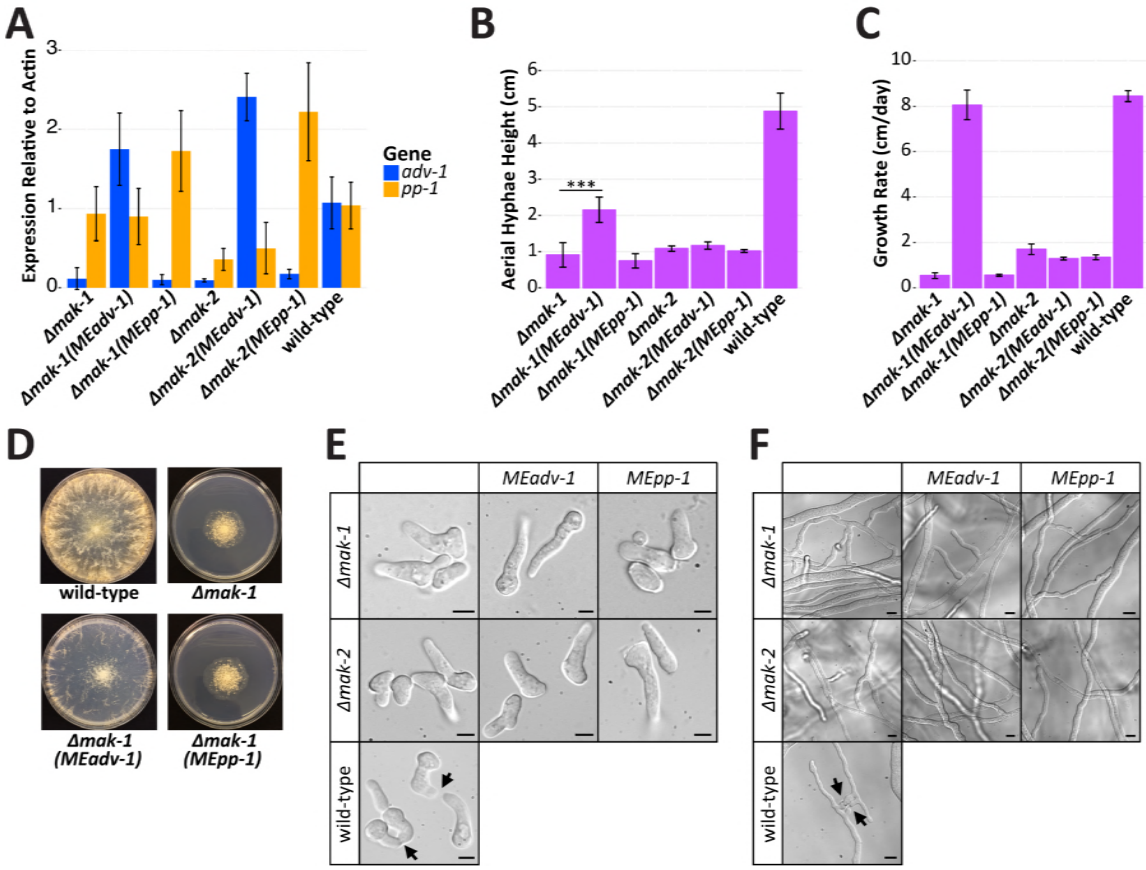

Figure 7. Misexpression of *adv-1* suppresses the growth phenotype of the *Δmak-1* mutant. **(A)** qRT-PCR data showing mRNA expression levels of *adv-1* and *pp-1* in *Δmak-1 (Ptef1-adv-1-v5; his-3 (MEadv-1))*, *Δmak-1 (Ptef1-pp-1-v5; his-3 (MEpp-1))*, *Δmak-2 (Ptef1-adv-1-v5; his-3 (MEadv-1))* and *Δmak-2 (Pccg1-pp-1-gfp; his-3 (MEpp-1))* strains compared to *Δmak-1*, *Δmak-2* and wild type cells. **(B)** Mean height of aerial hyphae of strains in (A) three days after inoculation (ANOVA+TukeyHSD, ***p=3.6E-8, n=6). **(C)** Mean growth rate per day of strains in (A) measured over 4 days (ANOVA+TukeyHSD, p<0.01, n=3). For all bar plots, error bars indicate standard deviation. **(D)** Colony morphology of the *Δmak-1* mutant relative to the wild-type strain and the *Δmak-1 (Ptef1-adv-1-v5; his-3 (MEadv-1))* and *Δmak-1 (Ptef1-pp-1-v5; his-3 (MEpp-1))* strains. **(E)** Photos showing a lack of germling fusion (scale bars = 5μm) or **(F)** hyphal fusion (scale bars =

bioRxiv preprint doi: https://doi.org/10.1101/281931; this version posted March 13, 2018. The copyright holder for this preprint (which was not certified by peer review) is the author/funder, who has granted bioRxiv a license to display the preprint in perpetuity. It is made available under aCC-BY-NC-ND 4.0 International license.

10μm) for each strains shown in (A). Arrows indicate chemotropic interactions in the wild-type strain.

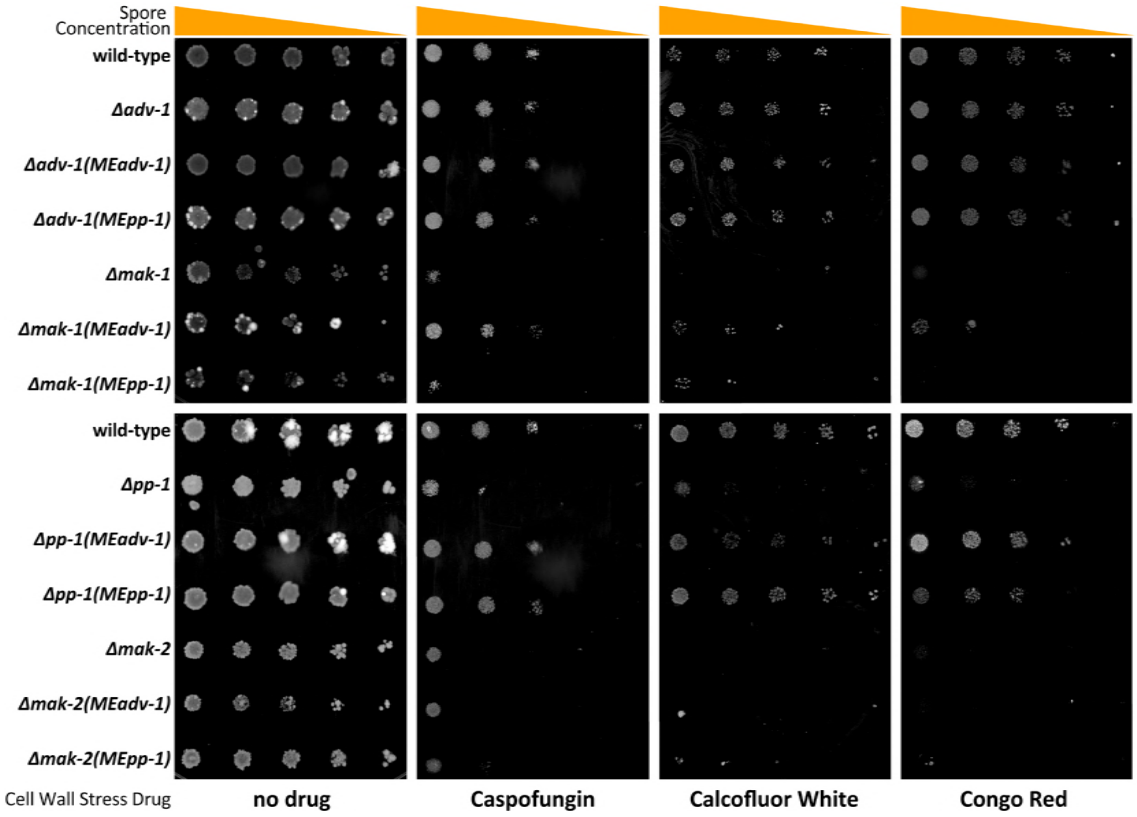

Figure 8. Misexpression of *adv-1* restores resistance to cell wall stress agents in *Δpp-1* and *Δmak-1* cells.

A 1:5 serial dilution from ~5000spores/spot to ~8spores/spot was performed on *Δpp-1 (Ptef1-adv-1-v5; his-3 (MEadv-1))*, *Δpp-1 (Ptef1-pp-1-v5; his-3 (MEpp-1))*, *Δmak-2 (Ptef1-adv-1-v5; his-3 (MEadv-1))*, *Δmak-2 (Pccg1-pp-1-gfp; his-3 (MEpp-1))*, *Δadv-1 (Ptef1-adv-1-v5; his-3 (MEadv-1))*, *Δadv-1 (Ptef1-pp-1-v5; his-3 (MEpp-1))*, *Δmak-1 (Ptef1-adv-1-v5; his-3 (MEadv-1))* and *Δmak-1 (Ptef1-pp-1-v5; his-3 (MEpp-1))* cells compared to *Δpp-1*, *Δadv-1*, *Δmak-1*, *Δmak-2*, and wild-type cells. All agar media contains VMM and FGS to force colonial growth. Plates were incubated at 30°C for 5 days. Drug concentrations: 1.3ug/mL caspofungin,

bioRxiv preprint doi: https://doi.org/10.1101/281931; this version posted March 13, 2018. The copyright holder for this preprint (which was not certified by peer review) is the author/funder, who has granted bioRxiv a license to display the preprint in perpetuity. It is made available under aCC-BY-NC-ND 4.0 International license.

1115 1.5mg/mL calcofluor white, and 1mg/mL congo red.

1116

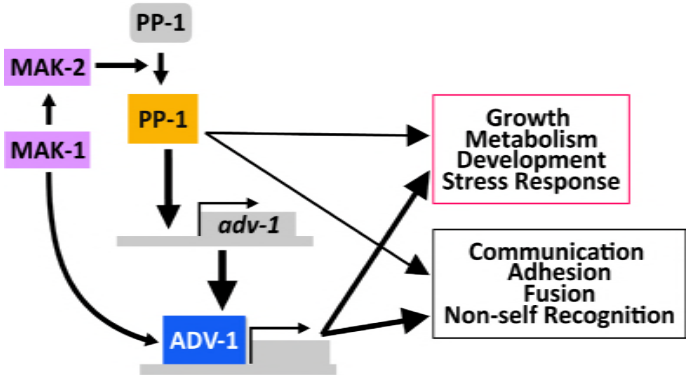

1117

1118 **Figure 9. Model for transcriptional regulation by MAK-1, MAK-2, PP-1 and**

1119 **ADV-1.** MAK-1 activates both MAK-2 and ADV-1-dependent transcription. MAK-2

1120 activates or de-represses PP-1, which is necessary for transcription of *adv-1* and other

1121 down-stream genes (inactivated PP-1 is grey, activated PP-1 is orange). PP-1 directly

1122 binds and regulates transcription of *adv-1*; ADV-1 is the direct transcriptional activator of

1123 many of the genes required for cell-to-cell communication, cell fusion, growth,

1124 development, and metabolism. Additionally, PP-1 and ADV-1 are important for

1125 mediating the cell wall stress response downstream of both MAK-1 and MAK-2. While

1126 our data indicates that ADV-1 is the primary regulatory for many downstream genes, PP-

1127 1 also contributes to the transcription of some of these genes independently of *adv-1*.

1128 Downstream gene groups are boxed with colors (magenta or black) that match the colors

1129 detailing the same groups in Figure 2.